Glucocorticoid receptor activation induces NK cells to produce AREG and restricts their anti-tumor activity in skin cancer

Qin Wei[1,2], Guirong Liang[1,2], Rui zeng[1], Yuancheng Li[1], Anlan Hong[1], Hongsheng Wang[1], Suying Feng[1], Yan Wang[1*], Yetao Wang[1,3*]

1 Hospital for Skin Diseases, Institute of Dermatology, Chinese Academy of Medical Sciences and Peking Union Medical College, Nanjing, China
2 These authors contributed equally
3 Lead Contact
*Correspondence: drwangyan@163.com; yetaowang@163.com

Summary

Natural killer (NK) cells are recognized as powerful anti-tumor effector cells, but their efficacy is often hindered by the tumor microenvironment (TME). In this study, we analyzed the single-cell transcriptome and cytokine production profiles of NK cells from 24 and 68 paired peri-tumor and tumor skin tissues, respectively. We found that NK cells within skin tumors downregulated anti-tumor cytokines IFN-γ and TNF-α while upregulating amphiregulin (AREG), an EGFR ligand that promotes tumor growth and immune tolerance. This cytokine shift was linked to increased activity of the glucocorticoid receptor (GR, encoded by NR3C1). We further demonstrated that glucocorticoids acting as natural ligands, specifically induced AREG production in NK cells, while NR3C1 knockout and its inhibitors abolished this effect. PGE2, prevalent in TMEs, promoted AREG production independently of glucocorticoid dosage. Moreover, GR activation induced a memory response in NK cells, enhancing AREG production upon subsequent stimuli by increasing chromatin accessibility around the AREG promoter. AREG knockout NK cells exhibited significantly enhanced tumor suppression in NCG mice inoculated with human melanoma or cutaneous squamous cell carcinoma cells. These findings highlight the therapeutic potential of targeting AREG production in NK cells for cancer treatment.

Keywords

NK cells, AREG, Glucocorticoid receptor, Skin cancer, Tumor microenvironment

Graphical abstract

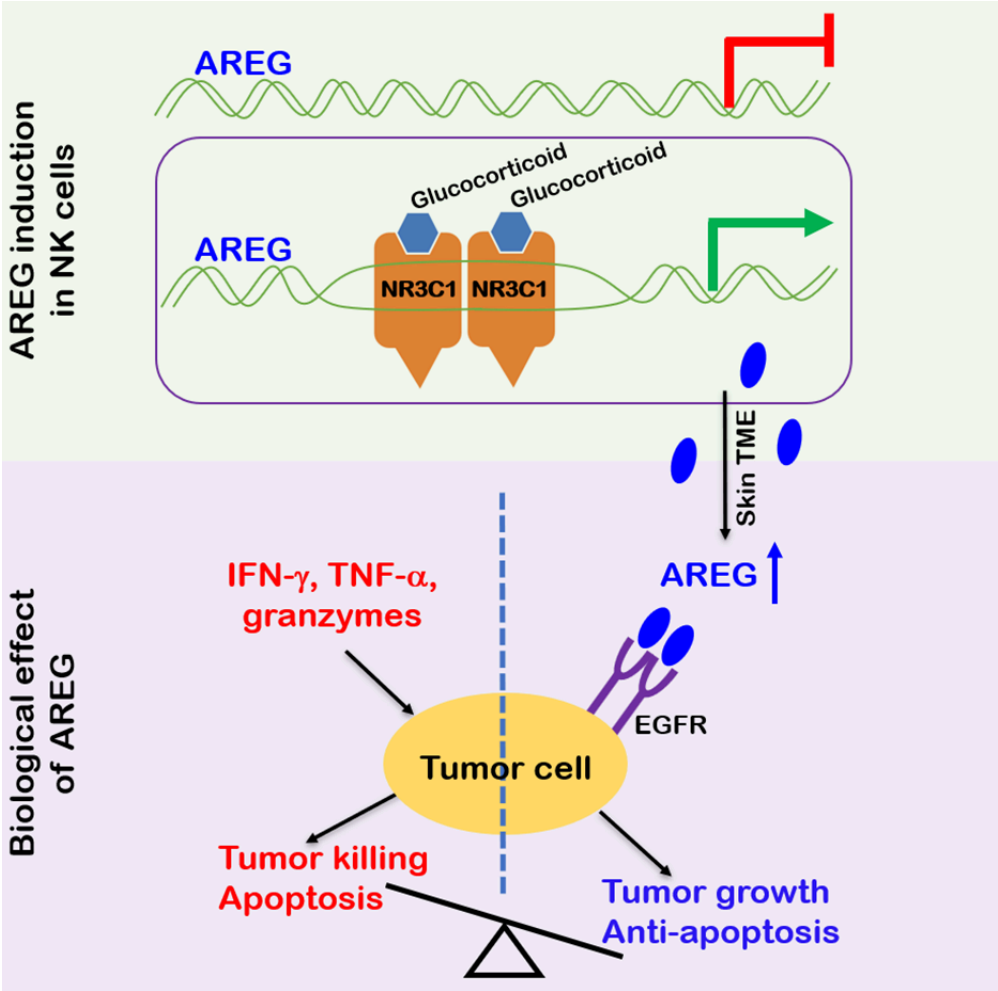

Introduction

Skin cancers are the most common human malignancies, including melanoma (MM) and non-melanoma skin cancers (NMSCs), the latter account for >90% of all skin cancers[1–3], mainly consist of basal cell carcinoma (BCC), cutaneous squamous cell carcinoma (cSCC) and extramammary paget disease (EMPD)[2,3]. While surgery remains effective treatment, immune therapies targeting PD-1 and CTLA-4 have shown promising clinical results in unresectable or metastatic/advanced BCC, cSCC and MM[3–6]. Tumor microenvironments (TMEs) play critical roles in responsiveness of checkpoint therapies. Unfavorable TMEs can lead to treatment resistance and poor prognosis[5,7], highlighting the need to identify determinants of unresponsive TMEs and associated biomarkers.

Natural killer (NK) cells play crucial roles in restraining tumor growth and metastasis by releasing perforin and granzymes, engaging death receptors, and producing anti-tumor cytokines such as IFN-γ and TNF-α[8]. Their adoptive transfer is not hindered by HLA restrictions and does not cause graft-versus-host disease. Various sources, including $CD34^+$ cells, iPSCs, peripheral blood, and cord blood, can be utilized for clinical NK cell preparation, making NK cells a focal point in tumor immunotherapy research[8,9].

On the one hand, NK cells significantly impact checkpoint therapy efficacy by modulating TMEs. For example, NK cells enhance the anti-PD-1 therapy response in melanoma by increasing intratumoral stimulatory dendritic cell abundance through FLT3LG production[7], while dysfunctional NK cell infiltration is linked to cSCC progression[10]. On the other hand, TMEs substantially impair NK cell anti-tumor function, limiting their effectiveness. Tumor hypoxia induces HIF1α to suppress IL-18-mediated activation and IFN-γ expression in NK cells[11]. Tumor-derived PGE2 impairs NK cell-produced XCL1 and CCL5, which are crucial for recruiting cDC1s for anti-tumor immunity[12]. Additionally, enhanced glucocorticoid receptor (GR, encoded by NR3C1) activity induces tumor cell PD-L1 expression, potentially inhibiting NK cell-mediated cytotoxicity[13,14]. Therefore, understanding the inhibitory mechanisms of NK cells within tumors is crucial for advancing NK cell-based immunotherapy.

Different from the known biological functions of NK cells, amphiregulin (AREG) is a ligand of epidermal growth factor receptor (EGFR), which plays important roles in promoting tumor growth and metastasis by enhancing cell survival, proliferation, angiogenesis and mediating immune tolerance[15–18]. The enhanced production of AREG in TME also contributes to therapeutic resistance, making AREG an attractive target for cancer therapies[17,19–21]. Our recent study revealed that unlike in mouse NK cells, the

chromatin region around AREG promoter is only accessible in human NK cells and AREG$^+$NK cells have a homeostatic function in HIV-1 induced inflammation[22]. However, the natural ligand responsible for inducing AREG in NK cells and the biological role of AREG produced by NK cells in their tumor-restricting effect remain unclear.

In this study, we conducted a comprehensive investigation into the transcriptome and biological function of NK cells in peri-tumor and tumor tissues from major types of skin cancer, including BCC, cSCC, EMPD, and acral melanoma (aMM). Our findings revealed that the activation of NR3C1, which induced NK cell AREG production and memory formation, represents a previously underappreciated counteracting mechanism for their anti-tumor function.

Results

NK cells are stable constituents of skin tumor lymphocytes

To examine the characteristics of NK cells among major types of skin cancer, we conducted a study using freshly isolated tumor and adjacent normal peri-tumor tissue from patients with BCC, cSCC, EMPD and aMM. These samples were subjected to single-cell transcriptome analysis and functional assessment (Figure 1A and Methods). We collected a total of 24 paired samples for single-cell RNA sequencing (scRNA-Seq) and 68 paired samples for flow cytometry analysis (Figures 1A, S1, and Table S1).

To ensure a more focused analysis of NK cells and minimize the presence of skin epithelial cells and fibroblasts[6,23], a CD45$^+$ cell enrichment step was employed prior to library preparation (Methods). Following filtering by Seurat and removal of non-hematopoietic cells, 146,643 CD45$^+$ cells were identified (Table S2 and Methods). Skin CD45$^+$ cells formed eight distinct clusters in uniform manifold approximation and projection (UMAP), representing NK cells, T cells, B cells, plasma blasts, dendritic cells, monophagocytes, mast cells, and neutrophils (Figures 1B and 1C). To confirm the identity of NK cells, we examined the expression of specific NK cell markers (NKG7, GZMB, GNLY, KLRD1, IFNG) and verified the absence of markers associated with other cell types (Figures 1C, 1D, and S2A)[22,24,25]. In total, 2,282 high-quality NK cells were identified based on these criteria.

Flow cytometry was utilized to validate the above results. To exclude T cells, B cells, monocytes/macrophages, dendritic cells, and other lineage-positive cells from the CD45 positive population, a panel of 14 lineage antibodies (CD3, CD4, TCRαβ, TCRγδ, CD19, CD20, CD22, CD34, FcεRIα, CD11c, CD303, CD123, CD1a, and CD14) was employed

(Figure 1E), NK cells were identified as $Lin^{-}TBX21^{+}$ cells based on previous studies [22,24,26]. The results demonstrated that NK cells constituted a significant population of lineage-negative cells in both tumor and peri-tumor tissues across the four types of skin cancer (Figure 1E). While the percentage of NK cells did not exhibit significant differences between tumor and peri-tumor tissues (Figure 1F), the numbers of NK cells were increased in the tumor tissue (Figure 1G), which aligns with the increased percentage and numbers of $CD45^{+}$ cells in the tumor (Figures 1H and 1I).

The common transcriptional features of NK cells in skin tumors

Compared to peri-tumor, the upregulated genes in skin tumor NK cells were enriched with responses to stress-associated pathways, such as HSF1-dependent transactivation and the HSP90 chaperone cycle for steroid hormone receptors (SHR) in the presence of ligand (HSPA1A, HSP90AA1, HSPA1B, DANJB1), as well as pathways related to IL-4 and IL-13 signaling (IL-4R, FOS, CEBPD, JUNB) (Figure 2A and Table S3). Notably, genes associated with regulated necrosis and interferon signaling (IFNG, GZMB, CASP4, IRF8, ISG20, IFITM1, IFITM3, GBP5), which restrict tumor growth, and genes associated with signaling by EGFR in cancer (AREG, UBC), which promote tumor growth, were both upregulated in skin tumor NK cells (Figure 2A and Table S3), indicating an inhibitory mechanism in the skin TMEs, which suppresses the anti-tumor activity of NK cells by upregulating AREG-EGFR signaling.

UMAP analysis revealed that NK cells from the skin peri-tumors and tumors grouped most strongly based on transcriptional characteristics rather than skin cancer types (Figures 2B, 2C, S2B and Table S4). Cluster 0 (C0) NK cells expressed markers similar to blood $CD56^{hi}$NK cells (IL2RA, IL7R, TCF7, BACH2, AREG)[22,24,27]. Cluster 1 NK cells expressed markers similar to blood $CD56^{dim}$NK cells (HAVCR2, FCGR3A, PRF1, CST7)[22,24]. Cluster 2 NK cells displayed high expression of AREG and genes related to tissue infiltrating (RGS1, CD69)[28], as well as AP-1 family members (JUN, ATF3 and FOSB). Clutter 3 NK cells highly expressed IFNG and TNF. Cluster 4 NK cells exhibited high expression of tissue resident marker CXCR6[28], and genes encoding GZMA, HLA-DRA, TIGIT and TNFRSF9. A minor population of NK cells in cluster 5 expressed interferon-stimulated genes but was not further analyzed due to their small number (25 cells) (Figures 2D and 2E).

Skin TME enhances NK cell AREG production

In contrast to mouse NK cells lacking AREG expression[22], transcriptional profiling of human NK cells in skin TMEs showed that these cells exhibit not only anti-tumor properties through IFNG and TNF expression, but also express AREG (Figure 2), which

plays pivotal roles in stimulating keratinocyte and fibroblast proliferation[29,30], inducing immune tolerance, promoting tumor growth[15–18], and contributing to therapeutic resistance against anti-cancer treatments[17,19–21]. Consequently, we investigated the production of both anti-tumor and pro-tumor cytokines by NK cells in skin TMEs.

The flow cytometry analysis revealed an upregulation in the production of AREG by skin tumor NK cells in comparison to their peri-tumor counterparts (Figures 3A and 3B). This finding aligns with the results obtained from previous RNA-Seq data shown in Figure 2A and Table S3. Conversely, the production of TNF-α by tumor NK cells was downregulated, while the production of IFN-γ remained unaltered (Figures 3A, 3C and 3D). The scRNA-Seq analysis indicated that the expression of AREG and IFNG or TNF was mutually exclusive in C0 and C3 NK cell clusters, while these cytokines were found to be co-expressed in the C2 NK cell cluster (Figure 2E). This expression pattern was subsequently validated by protein detection.

In skin tumors, the percentage of NK cells positive for AREG, including both $AREG^{+}IFN\text{-}\gamma^{-}$ and $AREG^{+}IFN\text{-}\gamma^{+}$ subsets, was increased (Figures 3E-3G). Conversely, NK cells that are negative for AREG but positive for IFN-γ ($AREG^{-}IFN\text{-}\gamma^{+}$) were decreased (Figures 3E and 3H). Similar trends were observed in the percentages of $AREG^{+}TNF\text{-}\alpha^{-}$ and $AREG^{-}TNF\text{-}\alpha^{+}$ NK cells in the skin tumor (Figures 3E and 3I-3K). Additionally, the percentage of AREG positive NK cells ($AREG^{+}IFN\text{-}\gamma^{-}$ and $AREG^{+}IFN\text{-}\gamma^{+}$) showed an inverse correlation with NK cells only positive for IFN-γ ($AREG^{-}IFN\text{-}\gamma^{+}$) (Figures 3L and 3M), while no significant correlation was found between the $AREG^{+}$ and $TNF\text{-}\alpha^{+}$ NK cell subsets (Figures 3N and 3O). These findings underscore the altered production of pro- and anti-tumor cytokines by NK cells in skin tumors.

Glucocorticoids are physiological ligands that stimulate NK cell AREG production

We tested 14 stimuli, including NK cell activating cytokines, ligands, antibodies, and combinations thereof, to pinpoint the physiological conditions inducing AREG production by NK cells. However, none of these stimuli induced detectable AREG in NK cells (Figure S3A). Comparison of gene expression profiles between $AREG^{+}$NK cells (C0, 2) and $AREG^{-}$NK cells (C1, 3, 4, 5) revealed consistently higher expression levels of glucocorticoid receptor (GR, NR3C1) target genes in $AREG^{+}$NK cells, along with increased GR activity (Figures 2E and 4A-4C)[31–34]. Furthermore, GR activity positively correlated with tumor stress (Figure 4D), suggesting a potential role for GR in responding to stress within skin TMEs. However, the GR activity did not correlate with NK cell activation signatures (Figure 4E), as evidenced by the lack of AREG induction under NK cell activating conditions (Figure S3A). Additionally, within skin tumors, AREG

expression was co-upregulated with GR target genes in AREG$^+$NK cells compared to their peri-tumor counterparts (Figure 4F). Notably, NR3C1 was uniquely upregulated in AREG$^+$NK cells (C0 or C2) from BCC, cSCC, and EMPD tumors (Figures S3B-S3E). Taken together, these findings suggest that NK cell AREG production may be induced by GR activation.

To validate the above hypothesis, peripheral blood mononuclear cells (PBMCs) were treated with dexamethasone (Dex), a synthetic glucocorticoid commonly used in anti-inflammation therapies. The results demonstrated a significant increase in AREG production by NK cells, while other cell types in the PBMCs did not exhibit the same response (Figures 4G, 4H and S4A). Similar results were observed when alternative glucocorticoids such as betamethasone and methylprednisolone were used (Figures S4B and S4C). It is worth noting that we observed a saturation effect of glucocorticoid treatment on NK cell AREG production. Across a range of glucocorticoid concentrations, from nanomolar to micromolar, all resulted in a similar percentage of AREG$^+$NK cells (Figure S4A-S4C). This implies that the lower concentration applied in our experimental setup was sufficient to activate NR3C1 in NK cells. Aligned with the preceding findings, a single NR3C1 binding site within the accessible chromatin region encompassing AREG promoter was identified in NK cells by JASPAR motif analysis (Figure 4I). Moreover, both Cas9/RNP-mediated NR3C1 knockout in NK cells and treatment with the NR3C1 antagonist Mifepristone (RU486) effectively suppressed Dex-induced AREG production by NK cells (Figure 4J-4L and S4D). Thus, glucocorticoids induced GR activation specifically stimulates AREG production in NK cells.

Glucocorticoids suppresses anti-tumor characteristics of NK cells

To comprehensively investigate the impact of GR activation on NK cells, we performed bulk RNA seq on NK cells in steady state or upon cytokine stimulation in the presence or absence of Dex. Initially, NK cells were sorted from untreated and Dex-treated PBMCs, followed by bulk RNA-Seq (Figure S5A). AREG exhibited the highest fold change in 102 Dex upregulated genes which enriched in response to steroid hormone (FKBP5, KLF9, CFLAR, TSC22D3)[32–34], and negative regulation of NK and T cell activation, cell proliferation, programmed cell death and apoptotic process (CFLAR, PRDM1, TSC22D3, TLE1, TNFAIP8, PIK3IP1, TXNIP, HPGD, PTGER2, ZFP36L2, CD55, FOXO1) (Figures 5A, S5B and Table S6)[33,35–43]. Many of these genes have been previously identified as targets of GR and have been implicated in conferring resistance to anti-tumor therapies. For example, PRDM1 reduces the sensitivity of NK cells to IL-2 and inhibits their production of IFN-γ and TNF-α[44–46]; TSC22D3 comprises anti-tumor therapy by blocking type I interferon response of DCs and activation of IFN-γ$^+$T cells[33]; TLE1 negatively regulates NK cell effector function and memory

response[24,37,38,47]; PTGER2, the receptor for PGE2, is essential in suppressing NK cell-derived XCL1 and CCL5, hindering cDC1 attraction, and compromising T cell-driven tumor control (Figure 5A and Table S6) [12,48,49].

In contrast, genes involved in response to type I and II interferon, positive regulation of TNF production, programmed cell death and apoptotic process were downregulated by Dex, including IFIT1, IFIT2, IFIT3, MX1, DDX58, IRF7, XCL2, STAT1, MYD88, RELB, TRAF1, TNFSF10, FASLG, IL-32, CD226, IL2RB, and IL15RA (Figures 5A, S5B and Table S6) [50,51]. Notably, many Dex downregulated genes play important roles in enhancing NK cell activation and tumor suppression (Figure 5A and Table S6). For instance, CD82 acts as a suppressor of cancer cell invasiveness[52]; Interferon-induced XAF1 promotes apoptosis of tumor cells[53,54]; The NK cell activating receptor CD226 promotes anti-tumor function by counteracting the negative regulatory effects of Dex-induced FOXO1 (Figure 5A and Table S6)[55]

NK cells were also sorted from PBMCs treated with IL-12+IL15+IL18 alone or in combination with Dex, followed by bulk RNA-Seq. Once again, AREG emerged with the highest fold change among the 80 Dex-upregulated genes in cytokine activated NK cells (Figure 5B and Table S6). A substantial overlap of Dex upregulated genes was observed between activated NK cells and their steady state counterparts (Figures 5A, 5B, S5C and Table S6). Dex downregulated genes were involved in inflammatory response, lymphocyte activation, co-stimulation, chemotaxis and anti-tumor activity of NK cells (CD44, TNF, LTA, LTB, CCL5, REL, TRAF1, GPR183, XCL1, XCL2, STAT5A, IL2RB, CD82, TNFRSF9) (Figures 5B, S5C and Table S6)[52,56–58]. Thus, in both steady and activated states, GR activation suppresses the anti-tumor traits of NK cells and fosters a pro-tumor profile, with the upregulation of AREG being the most representative signature.

PGE2 signaling enhances Dex-induced AREG production by NK cells

Tumor cell derived PGE2 plays crucial roles in mediating immune evasion by disturbing the communication and inducing dysfunction of conventional DCs, NK cells and cytotoxic T cells[12,48,49]. Additionally, the PGE2 metabolite 15-keto PGE2, enhances the immune suppressive activity of Tregs[59]. Our bulk RNA-Seq data revealed that human NK cells predominantly express PGE2 receptors PTGER2 and PTGER4, and Dex treatment specifically upregulates PTGER2 expression (Figure 5C). However, like PGE2, Dex also downregulated the NK cell expressed CCL5, XCL1, and XCL2, which are essential for recruiting cDC1s and facilitating the anti-tumor response (Figure 5D)[12]. We subsequently investigated the impact of PGE2 on NK cell AREG production.

Our experiment showed that PGE2 treatment alone failed to stimulate AREG production by NK cells (Figure S5D); nonetheless, it effectively enhanced Dex-induced AREG production in NK cells (Figure 5E). Inhibition of PTGER2 but not PTGER4 attenuated the effect of PGE2, and combined inhibition of PTGER2 and PTGER4 did not yield further suppression (Figure 5E). Inhibition of PTGER2 downstream components adenylate cyclase (AC) and CREB also suppressed PEG2 enhanced AREG production in NK cells upon Dex treatment (Figure 5E), indicating the involvement of the PGE2–PTGER2–cAMP–CREB pathway in augmenting GR activation-induced AREG production in NK cells. In contrast, the production of IFN-γ by NK cells induced by IL-12+IL15+IL18 remained unaffected by PGE2, both in the presence and absence of Dex (Figure 5F).

We further investigated the expression data of skin cutaneous melanoma (SKCM) from The Cancer Genome Atlas (TCGA, https://cancergenome.nih.gov/). The analysis showed that the expression of AREG and the expression of PTGS1 and PTGS2, which are responsible for PGE2 synthesis, were positively correlated in SKCM (Figure 5G). Moreover, the expression of AREG in SKCM positively correlated with GR-activated signatures but negatively correlated with GR-inhibited signatures in NK cells derived from our RNA-Seq data (Table S6 and Figure 5G).

GR activation alters NK cell chromatin accessibility and induces a memory-like response

Initial inflammatory cytokine treatment induced a memory-like response in NK cells, leading to elevated IFN-γ production and enhanced effectiveness against melanoma and leukemia[60–62]. We explored whether GR activation could uniquely induce a memory-like response in NK cells to potentiate their AREG production.

To evaluate this, NK cells from PBMCs were either initially activated with Dex or remained unstimulated. Both sets of NK cells were then allowed to rest for 5 days, with a low dose of IL-15 introduced to sustain NK cell viability. RNA-Seq and ATAC-Seq were performed on sorted NK cells after 16 hours of initial stimulation or after 5 days of rest to capture transcriptome and chromatin accessibility alterations associated with GR activation. Following secondary stimulation, AREG production was compared between the two groups (Figure 6A).

Our results showed that many genes induced by Dex after 16 hours were not differentially expressed after a 5-day rest (Figure 6B). Although AREG expression remained higher in the Dex-treated group after 5 days, the protein was undetectable, similar to NK cells without initial Dex stimulation (Figure S5E).

In contrast, the AREG promoter loci became more accessible to Tn5 transposase after 16 hours of Dex treatment, and this enhanced chromatin accessibility persisted after 5 days (Figure 6C). Similar patterns were observed for FKBP5 and TXNIP1, while DUSP1 and ZBTB16 accessibility returned to unstimulated levels (Figure 6C). ATAC-Seq showed that NR3C1 and PTGER2, important for AREG expression, their chromatin accessibility were unaffected by GR activation (Figure 6C and S5F). Thus, GR activation not only induced a temporary increase in AREG production in NK cells but also created long-lasting chromatin accessibility at the AREG loci when AREG protein was not detectable (Figure S5E). This suggests the potential establishment of a memory for AREG production.

Finally, flow cytometry results demonstrated that primarily Dex-stimulated NK cells consistently exhibited higher AREG production compared to their counterparts without primary stimulation (Figures 6D and 6E). However, the high concentration of IL-15 (50 ng/ml), which is crucial for the inflammatory cytokine-induced memory response of IFN-γ production in NK cells[24], did not alter the GR activation-induced memory response of AREG production in NK cells (Figure 6F).

The production of AREG by NK cells compromises their anti-tumor efficacy

As an EGFR ligand, AREG critically contributes to tumor progression and therapy resistance by enhancing tumor cell proliferation, survival, and immune evasion[15–21]. However, NK cells have traditionally been recognized as anti-tumor effector cells. To investigate whether NK cell AREG production affects their anti-tumor efficacy, we inoculated NCG mice (NOD/ShiLtJGpt-*Prkdc*^{em26Cd52}Il2rg^{em26Cd22}/*Gpt*) with cell lines derived from human melanoma or cSCC and evaluated the tumor restriction effect of wild-type or AREG knockout human NK cells (Figure 7A and S5G).

The results showed that intratumoral injection of wild-type NK cells effectively restricted the increase in tumor volume and weight following inoculation with the melanoma cell line A375 (Figures 7B-7D). Moreover, knockout of AREG in NK cells further enhanced their tumor restriction effect on A375 tumor growth (Figures 7E-7G). To determine whether this effect was also true for cSCC or other melanoma cell line-formed tumors, A431 and A2058 cells were inoculated into NCG mice. AREG knockout in NK cells also robustly boosted their anti-tumor function against A431 and A2058 tumor growth (Figures 7H-7M). Collectively, these results indicate that AREG expression in NK cells impairs their anti-tumor efficacy in skin tumors.

Furthermore, analysis of TCGA data revealed that high AREG expression correlates with poor prognosis in multiple cancers, including LUSC, HNSC, LUAD, LAML, LIHC, and PAAD (Figure S6). Conversely, high IFNG expression was not always associated with better prognosis in these cancers (Figure S6), suggesting that AREG expression may counteract the function of anti-tumor effectors.

Discussion

The use of NK cells for cancer treatment holds great promise. However, their effectiveness against solid tumors has been limited, hindering their clinical application. Research has focused on factors in the TMEs that inhibit NK cell activation and on methods to unleash their full cytotoxic potential, such as combining immune checkpoint blockade and in vitro generation of highly activated NK cells[8]. Our findings revealed that NK cells, in addition to killing tumors, can express AREG (Figure 3B)[22], a molecule that promotes tumor growth and induces immune tolerance[15–21]. The skin TMEs enhance AREG expression (Figure 3B), potentially explaining why NK cells are less effective against solid tumors.

We observed that in skin TMEs, the percentage of AREG$^+$ NK cells was negatively correlated with IFN-γ$^+$ NK cells, which did not produce AREG. Supporting this, none of the conditions that stimulate NK cell IFN-γ production and cytotoxicity induced AREG production (Figure S3A). Instead, GR signaling, which suppresses NK cell IFN-γ production and cytotoxicity, specifically induced AREG production (Figure 4H), suggesting antagonistic regulatory mechanisms for the anti-tumor and protumor functions of NK cells. Consistent with this, multiple genes upregulated in skin tumor NK cells overlapped with Dex-induced genes (Table S4 and Figure 4A). This was further supported by the observation that AREG expression levels in SKCM from TCGA data positively correlated with GR-activated NK cell signatures identified in our experiments (Figure 5E). Thus, inhibitors targeting GR signaling or the PGE2 pathway, which potentiates GR activity, should enhance NK cell anti-tumor activity.

The memory effect of pro-inflammatory cytokine-induced IFN-γ production in NK cells has been shown to effectively strengthen their anti-tumor activity[60–62]. However, primary GR activation induces sustained chromatin accessibility around the AREG promoter in NK cells, potentially contributing to a memory response for enhanced AREG production. This characteristic may lead to side effects of glucocorticoid treatment in cancer, such as therapeutic resistance and immune evasion[63,64], due to elevated AREG production and suppressed anti-tumor function of NK cells with repeated glucocorticoid use.

Our experiments showed that human NK cell transfer restricted the growth of tumors induced by human melanoma or cSCC cell lines in NCG mice. Notably, AREG knockout in NK cells further enhanced this restrictive effect (Figure 7), suggesting a new strategy of directly targeting AREG for NK cell-based cancer therapy. Similar experiments with cancer cells from other tissues should provide additional insights for this approach. Analysis of TCGA data revealed that high AREG expression consistently correlated with poor prognosis in LUSC, HNSC, LUAD, LAML, LIHC, and PAAD (Figure S6). In contrast, IFN-γ expression was associated with better prognosis only in LUSC and HNSC. This indicates that suppressing NK cell AREG production may offer a more effective anti-tumor strategy than boosting IFN-γ production.

Acknowledgments

This study was supported by CAMS Innovation Fund for Medical Sciences (CIFMS) (2024-I2M-3-005) and Hospital for Skin Diseases, Institute of Dermatology, Chinese Academy of Medical Sciences and Peking Union Medical College grant (3301030103119) to Yetao W., National key research and development program (2022YFC2504700, 2022YFC2504701, 2022YFC2504705) to Yan W., The open project of Jiangsu provincial science and technology resources (Clinical Resources) coordination service platform (TC2022B016), The Jiangsu provincial natural science funds for young scholars (SBK2023041928) and The young scientists fund of the national natural science foundation of China (82304236) to Y.L.. We thank the study participants who provided skin and blood samples. Wei Cheng, Hao Chen and Zhiming Chen assisted in acquiring skin cancer and histology pictures. All staff in the biobank of Institute of Dermatology, Chinese Academy of Medical Sciences, Jiangsu Biobank of Clinical Resources assisted with clinical sample collection. Guangzhou Genedenovo Biotechnology Co., Ltd assisted with sequencing data analysis.

Author contributions

Yetao Wang: Conceptualization; experiment design; data analysis; resources; supervision; validation; investigation; visualization; methodology; data curation; software; writing – original draft, review and editing; project administration; funding acquisition. Yan Wang: resources. Qin Wei: experiment design, performing experiments; data analysis; validation; visualization, data curation. Guirong Liang: performing experiments. Ruizeng: performing experiments; data analysis; validation. Yuancheng Li: data analysis; validation; visualization, software. Anlan Hong: resources. Hongsheng Wang: resources. Suying Feng: resources.

Declaration of interests

All authors declare no competing interests.

Figure legends

Figure 1. NK cells are stable constituents of skin tumor lymphocytes.

(A) Experimental design of this study.
(B) UMAP of skin tumor and peri-tumor $CD45^+$ lymphocytes.
(C) The expression of cell type specific markers for (B).
(D) The expression of NK cell and other cell type specific markers in the NK cell cluster.
(E) Flow cytometry of NK cells in tumor and peri-tumor of BCC, cSCC, EMPD and aMM.
(F) Percentage of NK cells in dermal $CD45^+$ cells from skin tumor and peri-tumor.
(G) Number of NK cells per million live dermal cells from skin tumor and peri-tumor.
(H) Percentage of dermal $CD45^+$ cells from skin tumor and peri-tumor.
(I) Number of $CD45^+$ cells per million live dermal cells from skin tumor and peri-tumor.
For (F-I) n=31, each dot represents a unique skin tumor donor (11 BCC, 14 cSCC, 4 EMPD and 2 aMM), Wilcoxon matched-pairs signed rank test, ns, not significant, data are mean with s.e.m.

Figure 2. Common transcriptional features of skin tumor and peri-tumor NK cells.

(A) Reactome analysis of tumor NK cells highly expressed genes.
(B) UMAP of re-clustered skin tumor and peri-tumor NK cells.
(C) Percentage of NK cell clusters in skin tumor and peri-tumor in different skin cancers.
(D) Dot plot displaying the signature genes in skin NK cell clusters.
(E) The expression of AREG, IFNG and TNF in NK cell clusters.

Figure 3. Skin tumor TME upregulates AREG production by NK cells.

(A) Skin dermal cells were stimulated with PMA and ionomycin for 3 hrs, the production of AREG, IFN-γ and TNF-α by NK cells ($CD45^+Lin^-TBX21^+$) were detected by flow cytometry. (B-D) Percentage of $AREG^+$ (C, n=23), TNF-α^+ (D, n=21) and IFN-γ^+ (E, n=23) NK cells in the tumor and peri-tumor detected in (A). (E) Flow cytometry of NK cells produced AREG vs IFN-γ or TNF-α in the tumor and peri-tumor. (F-K) Percentage of $AREG^+$IFN-γ^- (F), $AREG^+$IFN-γ^+ (G), $AREG^-$IFN-γ^+ (H) NK cells (n=23) and $AREG^+$TNF-α^- (I), $AREG^+$TNF-α^+ (J) and $AREG^-$TNF-α^+ (K) NK cells (n=21) detected in (E). (L, M) Correlation of $AREG^-$IFN-γ^+ with $AREG^+$IFN-γ^- (L) or with $AREG^+$IFN-γ^+ (M) dermal NK cells (n=46). (N, O) Correlation of $AREG^-$TNF-α^+ with $AREG^+$TNF-α^- (N) or with $AREG^+$TNF-α^+ (O) dermal NK cells (n=42).

For (B-D), (F-K), each dot represents a unique skin tumor donor, Wilcoxon matched-pairs signed rank test, data are mean with s.e.m., for (L-O), Spearman correlation, ns, not significant.

Figure 4. Glucocorticoid receptor activation induces NK cells AREG production.
(A, B) The average counts of AREG (A) and glucocorticoid target genes (B) between C1, 3, 4, 5 ($AREG^{-}$) and C0, 2 ($AREG^{+}$) NK cells. *P* value was determined by Seurat FindMarkers. (C) GR activity score between $AREG^{-}$ and $AREG^{+}$ NK cells. The gene set score was calculated by AddMouduleScore in Seurat, the P value was determined by Wilcoxon rank-sum test using R software. (D, E) Pearson correlation between GR activity score and tumor stress score (D) or NK cell activation score (E). (F) Average counts of GR target genes and AREG in skin tumor and peri-tumor $AREG^{+}$ NK cells. *P* value was determined by Seurat FindMarkers. (G) PMBCs were stimulated with Dex for 16 hrs, the production of AREG in indicated cell populations were detected by flow cytometry. (H) Percentage of $AREG^{+}$ cells in (G), n=8, two-tailed paired t-test. (I) Schematic map of AREG open chromatin region in NK cells (GES122548) and NR3C1 binding motif. (J) Control, AREG or NR3C1 knockout NK cells were stimulated with Dex for 16 hrs, their AREG production was detected by flow cytometry. (K) PBMCs were stimulated with Dex or Dex+GR inhibitor (RU486) for 16 hrs, the production of AREG by NK cells was detected by flow cytometry. (L) Percentage of $AREG^{+}$NK cells in (K), n=7, two-tailed paired t-test.

Figure 5. PGE2 signaling potentiates Dex induced AREG production in NK cells
(A) PBMCs were treated with or without Dex in RPMI for 16 hrs, $CD56^{dim}$NK cells were stored and were subjected to bulk RNA-Seq, the DEgenes were shown in volcano plot (Log_2FC> 0.5, *P*<0.01, determined by DESeq2, n=3). (B) As performed in (A), DEgenes of Dex treated or untreated NK cells in the condition of IL-12+IL-15+IL-18 stimulation were shown (n=3). (C, D) Normalized counts of indicated genes from (A) and (B). (E) PBMCs were untreated or incubated with PF-04418948 (PTGER2 inhibitor), L-161982 (PTGER4 inhibitor), SQ22536 (adenylate cyclase inhibitor) or 666-15 (CREB inhibitor) as indicated for 6 hrs, then were treated with Dex alone or together with PGE2 for 16 hrs, AREG production by NK cells were detected by flow cytometry. (F) PMBCs incubated with or without Dex were treated with IL-12+IL-15+IL-18 in the presence or absence of PGE2 for 16 hrs, IFN-γ production by NK cells were detected by flow cytometry. (G) Pearson correlation of AREG with PTGS1 or PTGS1 expression in SKCM from TCGA, and Pearson correlation of AREG expression in SKCM from TCGA with GR activated or inhibited NK cell signature derived from our RNA-Seq data. For (E), Wilcoxon matched-pairs signed rank test, for (F), two-tailed paired t-test. Data are mean with s.e.m., each dot represents one donor, ns, not significant.

Figure 6. GR activation induces memory-Like response in NK cells and enhances their AREG production

(A) Experimental schematic for detecting the effect of primary Dex treatment on the transcriptome, chromatin accessibility and AREG production of NK cells. (B) Expression of indicated genes in NK cells with or without primary Dex stimulation following a 5-day rest. *P* value was determined by DESeq2, n=4, ns, not significant. (C) ATAC-Seq analysis of sorted blood NK cells with or without primary Dex stimulation for 16 hrs, and after rest for 5 days. (D) PBMCs with and without primary Dex stimulation were stimulated with Dex after resting for 5 days, AREG production of NK cells were detected by flow cytometry. (E) The percentage of $AREG^{+}$NK cells detected in (D) (n=11). (F) The Dex primarily stimulated PBMCs were additionally treated with high concentration of IL-15 (50 ng/ml), the percentage of $AREG^{+}$NK cells were detected by flow cytometry (n=7). For (E, F), two-tailed paired t-test, each dot represents one donor, ns, not significant

Figure 7. AREG knockout in NK cells enhances their anti-tumor function.

(A) Skin cancer cell lines were inoculated subcutaneously in the axillary region of NCG mice. Wild type or AREG knockout NK cells were stimulated with IL-12, IL-15, and IL-18 for 16 hours before intratumoral injection on day 7 and 14 post-tumor inoculation. (B) A375 cells were inoculated into NCG mice and either injected intratumorally with 0.9% NaCl (vehicle) or wild-type NK cells as described in (A). On day 21, tumors from control and NK cell-treated mice were dissected, and tumor volume (C) and weight (D) were measured (n=5). (E-G), The experiment was performed as in (B), except NCG mice were treated with wild type NK cells (control) and AREG knockout NK cells (n=5). (H-M), The experiment was performed as in (E-G), except NCG mice were injected with A431 cells (n=5) (H-J) and A2085 cells (n=4) (K-M). For (C, F, I, L), Two-way ANOVA, for (D, G, J, M), Mann-Whitney test.

Methods

Key resources table

REAGENT or RESOURCE	SOURCE	IDENTIFIER
Antibodies		
Anti-Human CD3	Biolegend	Cat# 317306
Anti-Human CD4	Biolegend	Cat# 317408
Anti-Human TCRα/β	Biolegend	Cat# 306706
Anti-Human TCRγ/δ	Biolegend	Cat# 331208
Anti-Human CD19	Biolegend	Cat# 302206

Anti-Human CD20	Biolegend	Cat# 302304
Anti-Human CD22	Biolegend	Cat# 363508
Anti-Human CD14	Biolegend	Cat# 325604
Anti-Human CD34	ebioscience	Cat# 11-0349-42
Anti-Human FcεR1α	ebioscience	Cat# 11-5899-42
Anti-Human CD1a	Biolegend	Cat# 300104
Anti-Human CD11c	Biolegend	Cat# 301604
Anti-Human CD123	Biolegend	Cat# 306014
Anti-Human BDCA2	Biolegend	Cat# 354208
Anti-Human TBX21	ebioscience	Cat# 25-5825-82
Anti-Human IFN-γ	ebioscience	Cat# 17-7319-82
Anti-Human IFN-γ	ebioscience	Cat# 45-7319-42
Anti-Human TNF-α	ebioscience	Cat# 45-7349-42
Anti-Human AREG	ebioscience	Cat# 17-5370-42
Anti-Human CD45	ebioscience	Cat# 56-9459-42
Anti-Human CD56	Biolegend	Cat# 318306
Anti-Human CD56	BD	Cat# 564057
Biological Samples		
PBMCs	Jiangsu province blood center	https://www.jsblood.com.cn/
A375	ATCC	Cat# CRL-1619
A431	ATCC	Cat# CRL-1555
A2058	ATCC	Cat# CRL-3601
Chemicals, Peptides, and Recombinant Proteins		
IL-2	Novoprotein	Cat# C013
IL-12	Novoprotein	Cat# CI58
IL-15	Novoprotein	Cat# C016
IL-18	Novoprotein	Cat# CH29
IL-21	Novoprotein	Cat# CC45
4-1BBL	Novoprotein	Cat# CH04
MICA	Novoprotein	Cat# C489
Transferrin	Novoprotein	Cat# CJ41
IGF-I	Novoprotein	Cat# C032
IGF-II	Novoprotein	Cat# CF61
Insulin	Solarbio	Cat# I8830
PMA	Beyotime	Cat# S1819
Ionomycin	Beyotime	Cat# S1672

Mifepristone	MedChemExpress	Cat# HY-13683
Dexamethasone Sodium Phosphate Injection	Shiyao YINHU Pharmaceutical Co., Ltd.	Lot# 1022122362
Methylprednisolone Sodium Succinate	Sinopharm Ronshyn Pharmaceutical Co., Ltd.	LOT# 22101707
Compound Betamethasone Injection	Schering-Plough Labo N.V.	LOT# 00001473561
PF-04418948 (PTGER2 inhibitor)	MCE	Cat# HY-18966
L-161982 (PTGER4 inhibitor)	MCE	Cat# HY-108559
SQ22536 (adenylate cyclase inhibitor)	MCE	Cat# HY-100396
666-15 (CREB inhibitor)	MCE	Cat# HY-101120
Cell stimulation cocktail	ebioscience	Cat# 00-4970-03
Protein transport inhibitor	ebioscience	Cat# 00-4980-03
TRIzol reagent	Invitrogen	Cat# 15596026
RNAClean XP	Beckman Coulter	Cat# A63987
Alt-R S.p. Cas9 Nuclease V3	Integrated DNA Technologies	Cat# 1081059
ExoSAP-IT	Affymetrix	Cat# 78200
SuperScript™ III Reverse Transcriptase	Invitrogen	Cat# 18080-093
Fixable Viability Dye efluor 780	Invitrogen	Cat# 65-0865-18
Critical Commercial Assays		
Universal DNA purification kit	Tiangen	Cat# DP214-02
Blood genomic DNA isolation kit	Karroten	Cat# K2302
RNA fragmentation reagents	Invitrogen	AM8740
P3 Primary Cell 4D-NucleofectorTM X Kit S	Lonza	Cat# V4XP-3032
EasySep Human NK Cell Isolation Kit	STEMCELL	Cat# 17955
Hyperactive ATAC-Seq Library Prep Kit for Illumina	Vazyme	Cat# TD711
NK MACS Medium human	MACS	Cat# 130-114-429

Single Cell 3' Reagent Kits v3.1	10 X Genomics	Cat# PN-1000121
NEBNext Ultra II Non directional Second Strand Synthesis Module	NEB	Cat# E6111L
HiScribe T7 High Yield RNA Synthesis Kit	NEB	Cat# E2040S
Deposited Data		
	NCBI Gene Expression Omnibus	
Software and Algorithms		
FlowJo	FlowJo, LLC	https://www.flowjo.com/
GraphPad Prism	GraphPad Software, Inc	https://www.graphpad.com/scientific-software/prism/
Cell Ranger	10x Genomics	https://support.10xgenomics.com/single-cell-gene-expression/software/pipelines/latest/what-is-cell-ranger
SAMtools	Li H. et al.[65]	http://www.htslib.org
R Statistical Computing Software	The R Foundation	https://www.r-project.org/
JASPAR	JASPAR	http://jaspar.genereg.net
DESeq2	Love M. et al.[66]	https://bioconductor.org/packages/release/bioc/html/DESeq2.htmll
GSEA	Subramanian A. et al.[67]	https://www.gsea-msigdb.org/gsea/index.jsp
GSVA	Hänzelmann, S. et al.[68]	https://www.bioconductor.org/packages/release/bioc/html/GSVA.html
Seurat 3.0	Stuart T. et al.[69]	http://satijalab.org/seurat/
SCENIC	Aibar S. et al.[70]	https://github.com/aertslab/SCENIC
Cytoscape	Shannon P. et al.[71]	https://cytoscape.org/
Bowtie2	Langmead B. et al.[72]	https://bowtie-bio.sourceforge.net/bowtie2/index.shtml

CEL-Seq2	Hashimshony T. et al.[73]	https://github.com/yanailab/celseq2
MACS2	Zhang Y. et al.[74]	https://github.com/macs3-project/MACS/wiki/Install-macs2
Trimmomatic	Bolger A.et al. [75]	https://github.com/usadellab/Trimmomatic
IGVTools	Robinson J. et al. [76]	https://software.broadinstitute.org/software/igv/download

Resource availability

Further information and requests for resources and reagents should be directed to and will be fulfilled by the lead contact, Yetao Wang (yetaowang@163.com).

Materials availability

This study did not generate new unique reagents.

Data availability

The datasets produced in this study, including scRNA-Seq data of skin tumor and peri-tumor, and bulk RNA-Seq data of Dex treated and untreated NK cells for 16 hrs, are available in NCBI Gene Expression Omnibus (GEO) with accession number: GSE242941.

Bulk RNA-Seq data of Dex-primarily treated and untreated NK cells after 5 days of rest, and ATAC-Seq data of Dex-primarily treated and untreated NK cells after 16 hours and after 5 days of rest, are available in the NCBI Sequence Read Archive (SRA), BioProject: PRJNA1119074

Clinical samples

Skin tumor and peri-tumor samples were obtained from the biobank of Institute of Dermatology, Chinese Academy of Medical Sciences, Jiangsu Biobank of Clinical Resources (BM2015004). Blood samples were obtained from Jangsu province blood center. All participants provided written informed consent for protocols that were included in the study of cellular immunity in skin cancers, in accordance with procedures approved by the ethics committee of Institute of Dermatology, Chinese Academy of Medical Sciences and Peking Union Medical College. The clinical characteristics for each donor of skin cancer were provided in Figure S1 and Table S1 .

Human skin cell preparation

Isolation of dermal single cells from peri-tumor and tumor tissues for *in vitro* culture and flow cytometry: 1. After scraping off the subcutaneous fat tissue, skin biopsies were transferred to 1 ml dispase (5 U/mL in PBS containing 1% penicillin/streptomycin) and were incubated in 37°C for 2 hrs to separate epidermis from dermis; 2. Dermis was washed briefly in PBS and was transfer to dermis digestion solution (Collagenase III 3mg/ml + DNase (5 ug/ml) in 10% FBS/RPMI 1640) at 37°C for 2 hrs, shaking vigorously every 30 min; 3. The digested dermis was filtered through a 70 um strainer, the flow through was collected in a 15 ml tube, after centrifuge at 700 x g for 3min, the cells were resuspended in 500 ul MACS buffer (0.5% BSA and 2 mM EDTA in PBS), ready for use.

Isolation of skin $CD45^+$ cells for scRNA-Seq: Skin biopsies were digested according to the instruction of the whole skin dissociation kit (130-101-540, MACS). Briefly, after scraping off fat tissue, skin biopsies were cutted into small pieces (< 4 mm^2), each piece was digested with a buffer containing 435 ul buffer L, 12.5 ul enzyme P, 50 ul enzyme D and 2.5 ul enzyme A on 37°C shaker for 3 hrs. The digested skin tissue was diluted with ice cold DMEM containing 2% BSA, then was filtered through a 70 um strainer, the flow through was centrifuged at 300 x g for 10 min at 4°C. The isolated skin cells were resuspended in MACS buffer and were subjected to $CD45^+$ cell enrichment using magnetic beads (130-045-801, MACS).

Peripheral blood mononuclear cells (PBMCs) isolation

Each human peripheral blood leukopak was washed with 80 ml serum free RPMI 1640 (Gibco), and was overlaid on lymphoprep (STEMSELL, 07851), then was centrifuged at 500 x g for 30 min in room temperature. After washing with MACS buffer for 3 times, the isolated PBMCs were either used immediately or frozen in FBS containing 10% DMSO.

Flow cytometry

Skin cells or PBMCs were first stained with fixable viability dye efluor 780 (Invitrogen, 65-0865-18). For surface staining, cells were incubated in MACS buffer with antibodies at 4°C for 30 min in the dark. For intracellular staining, cells were fixed and permeabilized using Foxp3 staining kit (eBioscience, 00-5523-00), then cytokines or TBX21 were stained with antibodies in the permeabilization buffer at 4°C for 30 min in the dark. After washing with MACS buffer, the cells were ready for flow cytometry detection.

NK cell sorting

PBMCs were stained with fixable viability dye efluor 780, lineage antibodies (against CD3, CD4, TCRαβ, TCRγδ, CD19, CD20, CD22, CD34, FcεRIα, CD11c, CD303, CD123, CD1a, and CD14) and antibody against CD56. $CD56^{dim}$NK cells were sorted as

indicated in Figure S5A using BD FACSAria IIu. The sorted NK cells were subjected to bulk RNA-Seq and ATAC-Seq library preparation.

Cell culture and stimulation conditions

All cells were cultured at 37°C containing 5% CO_2.

Figures 3A-3K: Dermal cells were stimulated with PMA (81 nM) and ionomycin (1.34 uM) (1:500, eBioscience, 00-4970-03) in RPMI 1640 for 2 hrs.

Figures 4G and 4H: PBMCs were stimulated with Dex (100 nM) in RPMI 1640 for 16 hrs.

Figure 4J: After electroporation for 48 hrs, NK cells were stimulated with Dex (100 nM) in RPMI for 16 hrs.

Figures 4K and 4L: PBMCs were stimulated with Dex (100 nM) in the presence or absence of RU486 (100 nM) in RPMI 1640 for 16 hrs.

Figure 5E: PBMCs were pre-treated with PF-04418948 (5 μM), L-161982 (5 μM), SQ22536 (10 μM) or 666-15 (1 μM), or left untreated for 6 hours, then were treated with Dex (100 nM) alone or with PGE2 (1 μM) for 16 hours in RPMI 1640.

Figure 5F: PMBCs incubated with or without Dex (100 nM) were treated with IL-12 (10 ng/ml) + IL-15 (50 ng/ml) + IL-18 (50 ng/ml) in the presence or absence of PGE2 (1 uM) for 16 hrs in RPMI 1640.

Figure 6E: PBMCs with and without primary Dex (100 nM) stimulation were stimulated with Dex (100 nM) after resting for 5 days in RPMI 1640 containing 5 ng/ml IL-15.

Figure 6F: The culture conditions were the same as in Figure 6E, except that the Dex-primarily stimulated PBMCs were additionally treated with a high concentration of IL-15 (50 ng/ml).

scRNA-Seq library preparation

The scRNA-Seq libraries were prepared by Single Cell 3' Reagent Kits v3.1 (10 x Genomics, PN-1000121). The enriched skin $CD45^+$ cells were washed and resuspended in 1 x PBS containing 0.05% BSA. Cell number and viability were measured by trypan blue staining under microscope, cell concentration was adjusted to 1,000-1,500 cells/ul (viability > 90%). Single cell suspension was loaded onto Chromium Controller (10 x Genomics) to participate 8,000–10,000 single cells into gel beads in emulsions (GEMs). The quality of amplified cDNA and final sequencing library were measured by Agilent 2100 Expert (Agilent Technologies).The sequencing depth was controlled around 50,000 mean reads/cell. The libraries were sequenced by Illumina NovaSeq 6000.

Bulk RNA-Seq library preparation

The bulk RNA-Seq libraries of sorted Dex treated and untreated $CD56^{dim}$NK cells were prepared using CEL-Seq2[73]. Total RNA of sorted cells was extracted using TRIzol

reagent (ThermoFisher, 15596026). 100 ng RNA for each library was used for first strand cDNA synthesis using barcoded primers as follows (barcode underlined): Dex untreated repeat 1: 5'-GCCGGTAATACGACTCACTATAGGGAGTTCTACAGTCCGACGATCNNNNNNAGACTCTTTTTTTTTTTTTTTTTTTTTTTTTV-3'; Dex untreated repeat 2: 5'-GCCGGTAATACGACTCACTATAGGGAGTTCTACAGTCCGACGATCNNNNNNCATGAGTTTTTTTTTTTTTTTTTTTTTTTTTV-3'; Dex untreated repeat 3: 5'-GCCGGTAATACGACTCACTATAGGGAGTTCTACAGTCCGACGATCNNNNNNCAGATCTTTTTTTTTTTTTTTTTTTTTTTTTV-3'; Dex treated repeat 1: 5'-GCCGGTAATACGACTCACTATAGGGAGTTCTACAGTCCGACGATCNNNNNNAGCTAGTTTTTTTTTTTTTTTTTTTTTTTTTV-3'; Dex treated repeat 2: 5'-GCCGGTAATACGACTCACTATAGGGAGTTCTACAGTCCGACGATCNNNNNNCATGCATTTTTTTTTTTTTTTTTTTTTTTTTV-3'; Dex treated repeat 3: 5'-GCCGGTAATACGACTCACTATAGGGAGTTCTACAGTCCGACGATCNNNNNNTCACAGTTTTTTTTTTTTTTTTTTTTTTTTTV-3'; Cytokine stimulated, Dex untreated repeat 1: 5'-GCCGGTAATACGACTCACTATAGGGAGTTCTACAGTCCGACGATCNNNNNNAGCTCATTTTTTTTTTTTTTTTTTTTTTTTTV-3'; Cytokine stimulated, Dex untreated repeat 2: 5'-GCCGGTAATACGACTCACTATAGGGAGTTCTACAGTCCGACGATCNNNNNNCATGTCTTTTTTTTTTTTTTTTTTTTTTTTTV-3'; Cytokine stimulated, Dex untreated repeat 3: 5'-GCCGGTAATACGACTCACTATAGGGAGTTCTACAGTCCGACGATCNNNNNNAGGATCTTTTTTTTTTTTTTTTTTTTTTTTTV-3'; Cytokine stimulated, Dex treated repeat 1: 5'-GCCGGTAATACGACTCACTATAGGGAGTTCTACAGTCCGACGATCNNNNNNAGCTTCTTTTTTTTTTTTTTTTTTTTTTTTTV-3'; Cytokine stimulated, Dex treated repeat 2: 5'-GCCGGTAATACGACTCACTATAGGGAGTTCTACAGTCCGACGATCNNNNNNCACTAGTTTTTTTTTTTTTTTTTTTTTTTTTV-3'; Cytokine stimulated, Dex treated repeat 3: 5'-GCCGGTAATACGACTCACTATAGGGAGTTCTACAGTCCGACGATCNNNNNNAGTGCATTTTTTTTTTTTTTTTTTTTTTTTTV-3'. The second strand was synthesized using NEBNext Second Strand Synthesis Module (NEB, E6111L). The dsDNA was purified using RNAClean XP (Beckman Coulter, A63987) and was subjected to *in vitro* transcription (IVT) using HiScribe T7 High Yield RNA Synthesis Kit (NEB, E2040S). After ExoSAP-IT (Affymetrix, 78200) treatment, the IVT RNA was fragmented using RNA fragmentation reagents (Invitrogen, AM8740) and was subjected to the second round of reverse transcription using random hexamer: 5'-GCCTTGGCACCCGAGAATTCCANN NNNN-3' The final library was amplified with indexed primers: RP1: 5'-AATGATACGGCGACCACCGAGATCTACACGTTCAGAGTTCTACAGTCCGA-3' and RPI1: 5'-CAAGCAGAAGACGGCATACGAGATCGTGATGTGACTGGAGTTCCTTGGCACCCGAGAATTCCA-3'. After quality check, the purified libraries were sequenced by Illumina NovaSeq 6000.

ATAC-Seq library preparation

The ATAC-Seq library for NK cells was constructed using the Hyperactive ATAC-Seq Library Prep Kit for Illumina (Vazyme, TD711). Briefly, the nuclei of sorted NK cells were isolated using a lysis buffer. Fragmentation buffer with Tn5 transposase was added, and the mixture was incubated at 37°C for 30 minutes. The released DNA fragments were then purified using ATAC DNA extraction beads. The library was subsequently amplified and purified with ATAC DNA clean beads.

Cas9 RNP mediated knockout in NK cells

NK cells were isolated from PBMCs using EasySep human NK Cell isolation kit (STEMCELL, 17955) and were expanded in NK MACS medium (MACS, 130-114-429) for 10 days to render NK cells competent for electroporation. 200 pmol sgRNA (synthesized from GenScript) were mixed with 100 pmol Cas9 (IDT, 1081059) for 20 min in room temperature to form RNP. One million NK cells were resuspended in 20 ul 4D nucleofector master mix (82% P3 + 18% supplement 1; Lonza, V4XP-3032), and mixed with Cas9 RNP for electroporation using program CM137. The electroporated NK cells were ready for downstream experiments after culturing in NK MACS medium for 48 hrs. The target site for CD19 knockout (control) was 5'-CTAGGTCCGAAACATTCCAC-3'; for AREG knockout was 5'-GAGGACGGTTCACTACTAGA-3'; and for NR3C1 knockout was 5'-TTACATTGGTCGTACATGCA-3', the corresponding sgRNAs were synthesized from IDT.

scRNA-Seq data processing

An average 9043 cells per sample, 49,004 reads and 1243 median genes per cell were identified by cell ranger (10x Genomics, version 5.0.0) (Table S2). Following alignment, cells meeting the following criterias were retained using Seurat (Version 3.0) and were passed to downstream analysis: (1) nFeature range from 200 to 5900; (2) < 49000 UMIs; (3) < 35% UMIs of mitochondria genes. Potential doublets and multiplets were filtered by DoubletFinder, and 196,278 cells were integrated. The exclusive cell type specific markers were used to further exclude doublets and multiplets. CD45 negative non-hematopoietic cell clusters including keratinocytes (KRT1, KRT5, KRT10, KRT14), fibroblasts (MFAP5, PDPN, PDGFRA, COL1A1), endothelial cells (ACKR1, VWF, PECAM1) and pericytes (RGS5, ACTA2, TAGLN) were also excluded based on their cell type specific markers. Total 146,643 CD45 positive cells were re-clusterd into 8 unique clusters (res=0.5) and NK cell cluster was focused for further analysis.

To identify cluster highly expressed genes, the gene expression values for the cluster of interest was compared with the rest clusters using FindMarkers in Seurat by

Model-based Analysis of Single-cell Transcriptomics (MAST) test, the average counts for each cluster were calculated by AverageExpression function.

Gene sets score analysis

The AddModuleScore function in Seurat was used to calculate the gene set score of NK cell clusters, and the significance was determined by Wilcoxon rank-sum test. Signature genes that were used for gene sets score analysis were included in Table S5.

Gene set correlation analysis

The AUCell score of each gene set, including GR pathway activity, tumor stress or NK cell activity, in each cell were calculated, the correlation among gene sets was calculated by Pearson correlation. Cells with extreme values (count = 0) were discarded from the analysis.

Bulk RNA-Seq analysis

The transcriptome count matrix of all samples was generated using the default settings of CEL-Seq2 pipeline (https://github.com/yanailab/celseq2)[73]. Briefly, Read 2 was assigned to each sample based on their paired read 1 barcode and was mapped to hg19 using Bowie2. The UMIs for each sample were counted, and the generated count matrix was analyzed by DEseq2 package in R. The counts of transcripts per sample were normalized using variance stabilizing transformation (VST) method in DESeq2. The DEgenes were determined by DEseq2 ($Log_2FC > 0.5$, $P<0.01$).

ATAC-Seq analysis

Paired-end reads were filtered with Trimmomatic and aligned to the hg38 reference genome using Bowtie2. Duplicates were removed with Picard's MarkDuplicates. Each aligned read was trimmed to the first 9 bases at the 5' end to match the Tn5 transposase cut site. For peak smoothing, the start sites of trimmed reads were extended 10 bases upstream and downstream. Peaks were called with MACS2. Adjusted aligned reads were converted to TDF files for visualization using IGVTools.

Survival probability analysis

Survival and RNA-seq data from TCGA (The Cancer Genome Atlas) PanCancer project were extracted from the UCSC XENA database (https://xena.ucsc.edu/). The Survival package was to compute Kaplan Meier curves for each tumor and to calculate the log-rank test to obtain the survival probability.

Mouse experiments

All NCG mice (NOD/ShiLtJGpt-*Prkdc*^{em26Cd52}Il2rg^{em26Cd22}*/Gpt,* GemPharmatech, T001475) were kept in microisolator cages and provided with autoclaved food and

acidified, autoclaved water within a specific pathogen-free facility. The use of animals followed the guidelines of the Institutional Animal Care and Use Committee of the Hospital for Skin Diseases, Institute of Dermatology, Chinese Academy of Medical Sciences and Peking Union Medical College. All experimental protocols were reviewed and approved by this committee.

Statistical analysis

Statistical test was performed using GraphPad Prism 9. Wilcoxon matched-pairs signed rank test or two tailed paired t-test used in this study were specified in the figure legends. Variance was estimated by calculating the mean ± s.e.m. in each group. $P < 0.05$ was considered significant. For gene sets score analysis, the P value was determined by Wilcoxon rank-sum test using R software. $P < 0.05$ was considered significant.

Supplemental Figure legends

Figure S1. Histological pictures of skin cancer donors.

Selected histological pictures of skin cancer donors for BCC (n=13), cSCC (n=15), EMPD (n=6) and aMM (n=4).

Figure S2. Detection of NK cells by scRNA-Seq.

(A) The expression of markers for NK and other cell types in NK cells clusters.

(B) The distribution of NK cells from different skin tumor and peri-tumor donors.

Figure S3. Cluster unique DEgenes of NK cells in skin cancers

(A) PBMCs were stimulated in indicated conditions for 16 hrs, the AREG production from NK cells ($Lin^{-}TBX21^{+}$) were detected using flow cytometry. (B-E) NK cell cluster unique DEgenes in BCC (B), cSCC (C), EMPD (D) and aMM (E). DEgenes of tumor vs peri-tumor for each NK cell cluster were determined by Seurat FindAllMarkers ($P<0.05$, $Log_2FC>0.36$). The cluster unique DEgenes were selected by their Log_2FC value 1.5 fold higher than the other clusters.

Figure S4. Glucocorticoid stimulation induces NK cell AREG production.

(A-C) PBMCs were stimulated in different dose of dexamethasone (A), betamethasone (B) and methylprednisolone (C) for 16 hrs, the AREG production from NK cells ($Lin^{-}TBX21^{+}$) were detected using flow cytometry. (D) ICE analysis for knockout effect of AREG and NR3C1 in NK cells.

Figure S5. GR activation induces transcriptional alteration in NK cells.

(A) Purity check of NK cells before and after sorting. (B) Enriched pathways of Dex up (red) and down (blue) regulated genes by GO enrichment analysis (FDR<0.05). (C) Enriched pathways of Dex up (red) and down (blue) regulated genes in the condition of IL-12+IL-15+IL-18 stimulation by GO enrichment analysis (FDR<0.05). (D) PMBCs were treated with or without PGE2 for 16 hrs, AREG in the NK cell ($Lin^{-}TBX21^{+}$) was detected by flow cytometry. (E) PBMCs with or without primary Dex stimulation were cultured in low dose IL-15 for 5 days, before secondary Dex stimulation, the production of AREG by NK cells were detected by flow cytometry. (F) ATAC-Seq analysis of NR3C1 loci of sorted blood NK cells with or without primary Dex stimulation for 16 hrs, and after rest for 5 days. (G) Flow cytometry detection of AREG and IFN-γ in wild type and AREG knockout NK cells.

Figure S6. High AREG expression in cancers correlates with lower survival rates. The association of AREG or IFNG expression with the survival probability in different cancer types based on the TCGA database. HR (hazard ratio), Lung Squamous Cell Carcinoma (LUSC), Lung Adenocarcinoma (LUAD), Head-Neck Squamous Cell Carcinoma (HNSC), Acute myeloid leukemia (LAML), Liver Hepatocellular Carcinoma (LIHC), Pancreatic adenocarcinoma (PAAD).

References

1. Arnold, M., Singh, D., Laversanne, M., Vignat, J., Vaccarella, S., Meheus, F., Cust, A.E., de Vries, E., Whiteman, D.C., and Bray, F. (2022). Global Burden of Cutaneous Melanoma in 2020 and Projections to 2040. JAMA Dermatol. *158*, 495–503.

2. Henrikson, N.B., Ivlev, I., Blasi, P.R., Nguyen, M.B., Senger, C.A., Perdue, L.A., and Lin, J.S. (2023). Skin Cancer Screening: Updated Evidence Report and Systematic Review for the US Preventive Services Task Force. JAMA *329*, 1296–1307.

3. Tanese, K., Nakamura, Y., Hirai, I., and Funakoshi, T. (2019). Updates on the Systemic Treatment of Advanced Non-melanoma Skin Cancer. Front. Med. *6*, 160.

4. Stonesifer, C.J., Djavid, A.R., Grimes, J.M., Khaleel, A.E., Soliman, Y.S., Maisel-Campbell, A., Garcia-Saleem, T.J., Geskin, L.J., and Carvajal, R.D. (2021). Immune Checkpoint Inhibition in Non-Melanoma Skin Cancer: A Review of Current Evidence. Front. Oncol. *11*, 734354.

5. Jenkins, R.W., and Fisher, D.E. (2021). Treatment of Advanced Melanoma in 2020 and Beyond. J. Invest. Dermatol. *141*, 23–31.

6. Ji, A.L., Rubin, A.J., Thrane, K., Jiang, S., Reynolds, D.L., Meyers, R.M., Guo, M.G., George, B.M., Mollbrink, A., Bergenstråhle, J., et al. (2020). Multimodal Analysis of Composition and Spatial Architecture in Human Squamous Cell Carcinoma. Cell *182*, 1661–1662.

7. Barry, K.C., Hsu, J., Broz, M.L., Cueto, F.J., Binnewies, M., Combes, A.J., Nelson, A.E., Loo, K., Kumar, R., Rosenblum, M.D., et al. (2018). A natural killer–dendritic cell axis defines checkpoint therapy–responsive tumor microenvironments. Nat. Med. *24*, 1178–1191.

8. Laskowski, T.J., Biederstädt, A., and Rezvani, K. (2022). Natural killer cells in antitumour adoptive cell immunotherapy. Nat. Rev. Cancer *22*, 557–575.

9. Basar, R., Daher, M., and Rezvani, K. (2020). Next-generation cell therapies: the emerging role of CAR-NK cells. Hematology Am. Soc. Hematol. Educ. Program *2020*, 570–578.

10. Luci, C., Bihl, F., Bourdely, P., Khou, S., Popa, A., Meghraoui-Kheddar, A., Vermeulen, O., Elaldi, R., Poissonnet, G., Sudaka, A., et al. (2021). Cutaneous Squamous Cell Carcinoma Development Is Associated with a Temporal Infiltration of ILC1 and NK Cells with Immune Dysfunctions. J. Invest. Dermatol. *141*, 2369–2379.

11. Ni, J., Wang, X., Stojanovic, A., Zhang, Q., Wincher, M., Bühler, L., Arnold, A., Correia, M.P., Winkler, M., Koch, P.-S., et al. (2020). Single-Cell RNA Sequencing of Tumor-Infiltrating NK Cells Reveals that Inhibition of Transcription Factor HIF-1α Unleashes NK Cell Activity. Immunity *52*, 1075–1087.e8.

12. Böttcher, J.P., Bonavita, E., Chakravarty, P., Blees, H., Cabeza-Cabrerizo, M., Sammicheli, S., Rogers, N.C., Sahai, E., Zelenay, S., and Reis e Sousa, C. (2018). NK Cells Stimulate Recruitment of cDC1 into the Tumor Microenvironment Promoting Cancer Immune Control. Cell *172*, 1022–1037.e14.

13. Tian, D., Tian, M., Han, G., and Li, J.-L. (2019). Increased glucocorticoid receptor activity and proliferation in metastatic colon cancer. Sci. Rep. *9*, 11257.

14. Deng, Y., Xia, X., Zhao, Y., Zhao, Z., Martinez, C., Yin, W., Yao, J., Hang, Q., Wu, W., Zhang, J., et al. (2021). Glucocorticoid receptor regulates PD-L1 and MHC-I in pancreatic cancer cells to promote immune evasion and immunotherapy resistance. Nat. Commun. *12*, 7041.

15. Zaiss, D.M.W., Gause, W.C., Osborne, L.C., and Artis, D. (2015). Emerging functions of amphiregulin in orchestrating immunity, inflammation, and tissue repair. Immunity *42*, 216–226.

16. Wang, S., Zhang, Y., Wang, Y., Ye, P., Li, J., Li, H., Ding, Q., and Xia, J. (2016). Amphiregulin Confers Regulatory T Cell Suppressive Function and Tumor Invasion via the EGFR/GSK-3β/Foxp3 Axis. J. Biol. Chem. *291*, 21085–21095.

17. Xu, Q., Long, Q., Zhu, D., Fu, D., Zhang, B., Han, L., Qian, M., Guo, J., Xu, J., Cao, L., et al. (2019). Targeting amphiregulin (AREG) derived from senescent stromal cells diminishes cancer resistance and averts programmed cell death 1 ligand (PD-L1)-mediated immunosuppression. Aging Cell *18*, e13027.

18. Florentin, J., Zhao, J., Tai, Y.-Y., Sun, W., Ohayon, L.L., O'Neil, S.P., Arunkumar, A., Zhang, X., Zhu, J., Al Aaraj, Y., et al. (2022). Loss of Amphiregulin drives inflammation and endothelial apoptosis in pulmonary hypertension. Life Sci Alliance *5*. 10.26508/lsa.202101264.

19. Lindzen, M., Ghosh, S., Noronha, A., Drago, D., Nataraj, N.B., Leitner, O., Carvalho, S., Zmora, E., Sapoznik, S., Shany, K.B., et al. (2021). Targeting autocrine amphiregulin robustly and reproducibly inhibits ovarian cancer in a syngeneic model: roles for wildtype p53. Oncogene *40*, 3665–3679.

20. Hsieh, M.-J., Chen, Y.-H., Lee, I.-N., Huang, C., Ku, Y.-J., and Chen, J.-C. (2019). Secreted amphiregulin promotes vincristine resistance in oral squamous cell carcinoma. Int. J. Oncol. *55*, 949–959.

21. Ishikawa, N., Daigo, Y., Takano, A., Taniwaki, M., Kato, T., Hayama, S., Murakami, H., Takeshima, Y., Inai, K., Nishimura, H., et al. (2005). Increases of amphiregulin and transforming growth factor-alpha in serum as predictors of poor response to gefitinib among patients with advanced non-small cell lung cancers. Cancer Res. *65*, 9176–9184.

22. Wang, Y., Lifshitz, L., Silverstein, N.J., Mintzer, E., Luk, K., StLouis, P., Brehm, M.A., Wolfe, S.A., Deeks, S.G., and Luban, J. (2023). Transcriptional and chromatin profiling of human blood innate lymphoid cell subsets sheds light on HIV-1 pathogenesis. EMBO J., e114153.

23. Guerrero-Juarez, C.F., Lee, G.H., Liu, Y., Wang, S., Karikomi, M., Sha, Y., Chow, R.Y., Nguyen, T.T.L., Iglesias, V.S., Aasi, S., et al. (2022). Single-cell analysis of human basal cell carcinoma reveals novel regulators of tumor growth and the tumor microenvironment. Sci Adv *8*, eabm7981.

24. Wang, Y., Lifshitz, L., Gellatly, K., Vinton, C.L., Busman-Sahay, K., McCauley, S., Vangala, P., Kim, K., Derr, A., Jaiswal, S., et al. (2020). HIV-1-induced cytokines deplete homeostatic innate lymphoid cells and expand TCF7-dependent memory NK cells. Nat. Immunol. *21*, 274–286.

25. Reynolds, G., Vegh, P., Fletcher, J., Poyner, E.F.M., Stephenson, E., Goh, I., Botting, R.A., Huang, N., Olabi, B., Dubois, A., et al. (2021). Developmental cell programs are co-opted in inflammatory skin disease. Science *371*. 10.1126/science.aba6500.

26. Bal, S.M., Golebski, K., and Spits, H. (2020). Plasticity of innate lymphoid cell subsets. Nat. Rev. Immunol. *20*, 552–565.

27. Collins, P.L., Cella, M., Porter, S.I., Li, S., Gurewitz, G.L., Hong, H.S., Johnson, R.P., Oltz, E.M., and Colonna, M. (2019). Gene Regulatory Programs Conferring Phenotypic Identities to Human NK Cells. Cell *176*, 348–360.e12.

28. Tang, F., Li, J., Qi, L., Liu, D., Bo, Y., Qin, S., Miao, Y., Yu, K., Hou, W., Li, J., et al. (2023). A pan-cancer single-cell panorama of human natural killer cells. Cell *0*. 10.1016/j.cell.2023.07.034.

29. Stoll, S.W., Stuart, P.E., Lambert, S., Gandarillas, A., Rittié, L., Johnston, A., and Elder, J.T. (2016). Membrane-Tethered Intracellular Domain of Amphiregulin Promotes Keratinocyte Proliferation. J. Invest. Dermatol. *136*, 444–452.

30. Zhao, X., Yang, W., Yu, T., Yu, Y., Cui, X., Zhou, Z., Yang, H., Yu, Y., Bilotta, A.J., Yao, S., et al. (2023). Th17 Cell-Derived Amphiregulin Promotes Colitis-Associated Intestinal Fibrosis Through Activation of mTOR and MEK in Intestinal Myofibroblasts. Gastroenterology *164*, 89–102.

31. Wang, J.-C., Derynck, M.K., Nonaka, D.F., Khodabakhsh, D.B., Haqq, C., and Yamamoto, K.R. (2004). Chromatin immunoprecipitation (ChIP) scanning identifies primary glucocorticoid receptor target genes. Proc. Natl. Acad. Sci. U. S. A. *101*, 15603–15608.

32. Mostafa, M.M., Rider, C.F., Shah, S., Traves, S.L., Gordon, P.M.K., Miller-Larsson, A., Leigh, R., and Newton, R. (2019). Glucocorticoid-driven transcriptomes in human airway epithelial cells: commonalities, differences and functional insight from cell lines and primary cells. BMC Med. Genomics *12*, 29.

33. Yang, H., Xia, L., Chen, J., Zhang, S., Martin, V., Li, Q., Lin, S., Chen, J., Calmette, J., Lu, M., et al. (2019). Stress–glucocorticoid–TSC22D3 axis compromises therapy-induced antitumor immunity. Nat. Med. *25*, 1428–1441.

34. Obradović, M.M.S., Hamelin, B., Manevski, N., Couto, J.P., Sethi, A., Coissieux, M.-M., Münst, S., Okamoto, R., Kohler, H., Schmidt, A., et al. (2019). Glucocorticoids promote breast cancer metastasis. Nature *567*, 540–544.

35. Uche, U.U., Piccirillo, A.R., Kataoka, S., Grebinoski, S.J., D'Cruz, L.M., and Kane, L.P. (2018). PIK3IP1/TrIP restricts activation of T cells through inhibition of PI3K/Akt. J. Exp. Med. *215*, 3165–3179.

36. Chen, S., Bonifati, S., Qin, Z., St Gelais, C., Kodigepalli, K.M., Barrett, B.S., Kim, S.H., Antonucci, J.M., Ladner, K.J., Buzovetsky, O., et al. (2018). SAMHD1 suppresses innate immune responses to viral infections and inflammatory stimuli by inhibiting the NF-κB and interferon pathways. Proc. Natl. Acad. Sci. U. S. A. *115*, E3798–E3807.

37. Ramasamy, S., Saez, B., Mukhopadhyay, S., Ding, D., Ahmed, A.M., Chen, X., Pucci, F., Yamin, R. 'e, Wang, J., Pittet, M.J., et al. (2016). Tle1 tumor suppressor negatively regulates inflammation in vivo and modulates NF-κB inflammatory pathway. Proc. Natl. Acad. Sci. U. S. A. *113*, 1871–1876.

38. Chodaparambil, J.V., Pate, K.T., Hepler, M.R.D., Tsai, B.P., Muthurajan, U.M., Luger, K., Waterman, M.L., and Weis, W.I. (2014). Molecular functions of the TLE tetramerization domain in Wnt target gene repression. EMBO J. *33*, 719–731.

39. Kim, D.O., Byun, J.-E., Kim, W.S., Kim, M.J., Choi, J.H., Kim, H., Choi, E., Kim, T.-D., Yoon, S.R., Noh, J.-Y., et al. (2020). TXNIP Regulates Natural Killer Cell-Mediated Innate Immunity by Inhibiting IFN-γ Production during Bacterial Infection. Int. J. Mol. Sci. *21*. 10.3390/ijms21249499.

40. Park, A., Lee, Y., Kim, M.S., Kang, Y.J., Park, Y.-J., Jung, H., Kim, T.-D., Lee, H.G., Choi, I., and Yoon, S.R. (2018). Prostaglandin E2 Secreted by Thyroid Cancer Cells Contributes to Immune Escape Through the Suppression of Natural Killer (NK) Cell Cytotoxicity and NK Cell Differentiation. Front. Immunol. *9*, 1859.

41. Cook, M.E., Bradstreet, T.R., Webber, A.M., Kim, J., Santeford, A., Harris, K.M., Murphy, M.K., Tran, J., Abdalla, N.M., Schwarzkopf, E.A., et al. (2022). The ZFP36 family of RNA binding proteins regulates homeostatic and autoreactive T cell responses. Sci Immunol *7*, eabo0981.

42. Bellone, S., Roque, D., Cocco, E., Gasparrini, S., Bortolomai, I., Buza, N., Abu-Khalaf, M., Silasi, D.-A., Ratner, E., Azodi, M., et al. (2012). Downregulation of membrane complement

inhibitors CD55 and CD59 by siRNA sensitises uterine serous carcinoma overexpressing Her2/neu to complement and antibody-dependent cell cytotoxicity in vitro: implications for trastuzumab-based immunotherapy. Br. J. Cancer *106*, 1543–1550.

43. Deng, Y., Kerdiles, Y., Chu, J., Yuan, S., Wang, Y., Chen, X., Mao, H., Zhang, L., Zhang, J., Hughes, T., et al. (2015). Transcription factor Foxo1 is a negative regulator of natural killer cell maturation and function. Immunity *42*, 457–470.

44. Akman, B., Hu, X., Liu, X., Hatipoğlu, T., You, H., Chan, W.C., and Küçük, C. (2021). PRDM1 decreases sensitivity of human NK cells to IL2-induced cell expansion by directly repressing CD25 (IL2RA). J. Leukoc. Biol. *109*, 901–914.

45. Smith, M.A., Maurin, M., Cho, H.I., Becknell, B., Freud, A.G., Yu, J., Wei, S., Djeu, J., Celis, E., Caligiuri, M.A., et al. (2010). PRDM1/Blimp-1 controls effector cytokine production in human NK cells. J. Immunol. *185*, 6058–6067.

46. Franco, L.M., Gadkari, M., Howe, K.N., Sun, J., Kardava, L., Kumar, P., Kumari, S., Hu, Z., Fraser, I.D.C., Moir, S., et al. (2019). Immune regulation by glucocorticoids can be linked to cell type-dependent transcriptional responses. J. Exp. Med. *216*, 384–406.

47. Bergeron, B.P., Barnett, K.R., Bhattarai, K.R., Mobley, R.J., Hansen, B.S., Brown, A., Kodali, K., High, A.A., Jeha, S., Pui, C.-H., et al. (2023). Mutual antagonism between glucocorticoid and canonical Wnt signaling pathways in B-cell acute lymphoblastic leukemia. Blood Adv. 10.1182/bloodadvances.2022009498.

48. Bayerl, F., Meiser, P., Donakonda, S., Hirschberger, A., Lacher, S.B., Pedde, A.-M., Hermann, C.D., Elewaut, A., Knolle, M., Ramsauer, L., et al. (2023). Tumor-derived prostaglandin E2 programs cDC1 dysfunction to impair intratumoral orchestration of anti-cancer T cell responses. Immunity *56*, 1341–1358.e11.

49. Zelenay, S., van der Veen, A.G., Böttcher, J.P., Snelgrove, K.J., Rogers, N., Acton, S.E., Chakravarty, P., Girotti, M.R., Marais, R., Quezada, S.A., et al. (2015). Cyclooxygenase-Dependent Tumor Growth through Evasion of Immunity. Cell *162*, 1257–1270.

50. Liu, S.-Y., Sanchez, D.J., Aliyari, R., Lu, S., and Cheng, G. (2012). Systematic identification of type I and type II interferon-induced antiviral factors. Proc. Natl. Acad. Sci. U. S. A. *109*, 4239–4244.

51. Platanias, L.C. (2005). Mechanisms of type-I- and type-II-interferon-mediated signalling. Nat. Rev. Immunol. *5*, 375–386.

52. Liu, W.M., and Zhang, X.A. (2006). KAI1/CD82, a tumor metastasis suppressor. Cancer Lett. *240*, 183–194.

53. Jeong, S.-I., Kim, J.-W., Ko, K.-P., Ryu, B.-K., Lee, M.-G., Kim, H.-J., and Chi, S.-G. (2018). XAF1 forms a positive feedback loop with IRF-1 to drive apoptotic stress response and suppress tumorigenesis. Cell Death Dis. *9*, 806.

54. Yang, R., Sun, L., Li, C.-F., Wang, Y.-H., Yao, J., Li, H., Yan, M., Chang, W.-C., Hsu, J.-M., Cha, J.-H., et al. (2021). Galectin-9 interacts with PD-1 and TIM-3 to regulate T cell death and is a target for cancer immunotherapy. Nat. Commun. *12*, 832.

55. Du, X., de Almeida, P., Manieri, N., de Almeida Nagata, D., Wu, T.D., Harden Bowles, K., Arumugam, V., Schartner, J., Cubas, R., Mittman, S., et al. (2018). CD226 regulates natural killer cell antitumor responses via phosphorylation-mediated inactivation of transcription factor FOXO1. Proc. Natl. Acad. Sci. U. S. A. *115*, E11731–E11740.

56. Galandrini, R., De Maria, R., Piccoli, M., Frati, L., and Santoni, A. (1994). CD44 triggering enhances human NK cell cytotoxic functions. J. Immunol. *153*, 4399–4407.

57. Wu, S.-Y., Fu, T., Jiang, Y.-Z., and Shao, Z.-M. (2020). Natural killer cells in cancer biology and therapy. Mol. Cancer *19*, 120.

58. Brownlie, D., Scharenberg, M., Mold, J.E., Hård, J., Kekäläinen, E., Buggert, M., Nguyen, S., Wilson, J.N., Al-Ameri, M., Ljunggren, H.-G., et al. (2021). Expansions of adaptive-like NK cells with a tissue-resident phenotype in human lung and blood. Proc. Natl. Acad. Sci. U. S. A. *118*. 10.1073/pnas.2016580118.

59. Schmidleithner, L., Thabet, Y., Schönfeld, E., Köhne, M., Sommer, D., Abdullah, Z., Sadlon, T., Osei-Sarpong, C., Subbaramaiah, K., Copperi, F., et al. (2019). Enzymatic Activity of HPGD in Treg Cells Suppresses Tconv Cells to Maintain Adipose Tissue Homeostasis and Prevent Metabolic Dysfunction. Immunity *50*, 1232–1248.e14.

60. Marin, N.D., Krasnick, B.A., Becker-Hapak, M., Conant, L., Goedegebuure, S.P., Berrien-Elliott, M.M., Robbins, K.J., Foltz, J.A., Foster, M., Wong, P., et al. (2021). Memory-like Differentiation Enhances NK Cell Responses to Melanoma. Clin. Cancer Res. *27*, 4859–4869.

61. Berrien-Elliott, M.M., Cashen, A.F., Cubitt, C.C., Neal, C.C., Wong, P., Wagner, J.A., Foster, M., Schappe, T., Desai, S., McClain, E., et al. (2020). Multidimensional Analyses of Donor Memory-Like NK Cells Reveal New Associations with Response after Adoptive Immunotherapy for Leukemia. Cancer Discov. *10*, 1854–1871.

62. Bednarski, J.J., Zimmerman, C., Berrien-Elliott, M.M., Foltz, J.A., Becker-Hapak, M., Neal, C.C., Foster, M., Schappe, T., McClain, E., Pence, P.P., et al. (2022). Donor memory-like NK cells persist and induce remissions in pediatric patients with relapsed AML after transplant. Blood *139*, 1670–1683.

63. Kalfeist, L., Galland, L., Ledys, F., Ghiringhelli, F., Limagne, E., and Ladoire, S. (2022). Impact of Glucocorticoid Use in Oncology in the Immunotherapy Era. Cells *11*. 10.3390/cells11050770.

64. Narayanan, S., Srinivas, S., and Feldman, D. (2016). Androgen-glucocorticoid interactions in the era of novel prostate cancer therapy. Nat. Rev. Urol. *13*, 47–60.

65. Li, H., Handsaker, B., Wysoker, A., Fennell, T., Ruan, J., Homer, N., Marth, G., Abecasis, G., Durbin, R., and 1000 Genome Project Data Processing Subgroup (2009). The Sequence Alignment/Map format and SAMtools. Bioinformatics *25*, 2078–2079.

66. Love, M.I., Huber, W., and Anders, S. (2014). Moderated estimation of fold change and dispersion for RNA-seq data with DESeq2. Genome Biol. *15*, 550.

67. Subramanian, A., Tamayo, P., Mootha, V.K., Mukherjee, S., Ebert, B.L., Gillette, M.A., Paulovich, A., Pomeroy, S.L., Golub, T.R., Lander, E.S., et al. (2005). Gene set enrichment

analysis: a knowledge-based approach for interpreting genome-wide expression profiles. Proc. Natl. Acad. Sci. U. S. A. *102*, 15545–15550.

68. Hänzelmann, S., Castelo, R., and Guinney, J. (2013). GSVA: gene set variation analysis for microarray and RNA-seq data. BMC Bioinformatics *14*, 7.

69. Stuart, T., Butler, A., Hoffman, P., Hafemeister, C., Papalexi, E., Mauck, W.M., 3rd, Hao, Y., Stoeckius, M., Smibert, P., and Satija, R. (2019). Comprehensive Integration of Single-Cell Data. Cell *177*, 1888–1902.e21.

70. Aibar, S., González-Blas, C.B., Moerman, T., Huynh-Thu, V.A., Imrichova, H., Hulselmans, G., Rambow, F., Marine, J.-C., Geurts, P., Aerts, J., et al. (2017). SCENIC: single-cell regulatory network inference and clustering. Nat. Methods *14*, 1083–1086.

71. Shannon, P., Markiel, A., Ozier, O., Baliga, N.S., Wang, J.T., Ramage, D., Amin, N., Schwikowski, B., and Ideker, T. (2003). Cytoscape: a software environment for integrated models of biomolecular interaction networks. Genome Res. *13*, 2498–2504.

72. Langmead, B., and Salzberg, S.L. (2012). Fast gapped-read alignment with Bowtie 2. Nat. Methods *9*, 357–359.

73. Hashimshony, T., Senderovich, N., Avital, G., Klochendler, A., de Leeuw, Y., Anavy, L., Gennert, D., Li, S., Livak, K.J., Rozenblatt-Rosen, O., et al. (2016). CEL-Seq2: sensitive highly-multiplexed single-cell RNA-Seq. Genome Biol. *17*, 77.

74. Zhang, Y., Liu, T., Meyer, C.A., Eeckhoute, J., Johnson, D.S., Bernstein, B.E., Nusbaum, C., Myers, R.M., Brown, M., Li, W., et al. (2008). Model-based analysis of ChIP-Seq (MACS). Genome Biol. *9*, R137.

75. Bolger, A.M., Lohse, M., and Usadel, B. (2014). Trimmomatic: a flexible trimmer for Illumina sequence data. Bioinformatics *30*, 2114–2120.

76. Robinson, J.T., Thorvaldsdóttir, H., Winckler, W., Guttman, M., Lander, E.S., Getz, G., and Mesirov, J.P. (2011). Integrative genomics viewer. Nat. Biotechnol. *29*, 24–26.

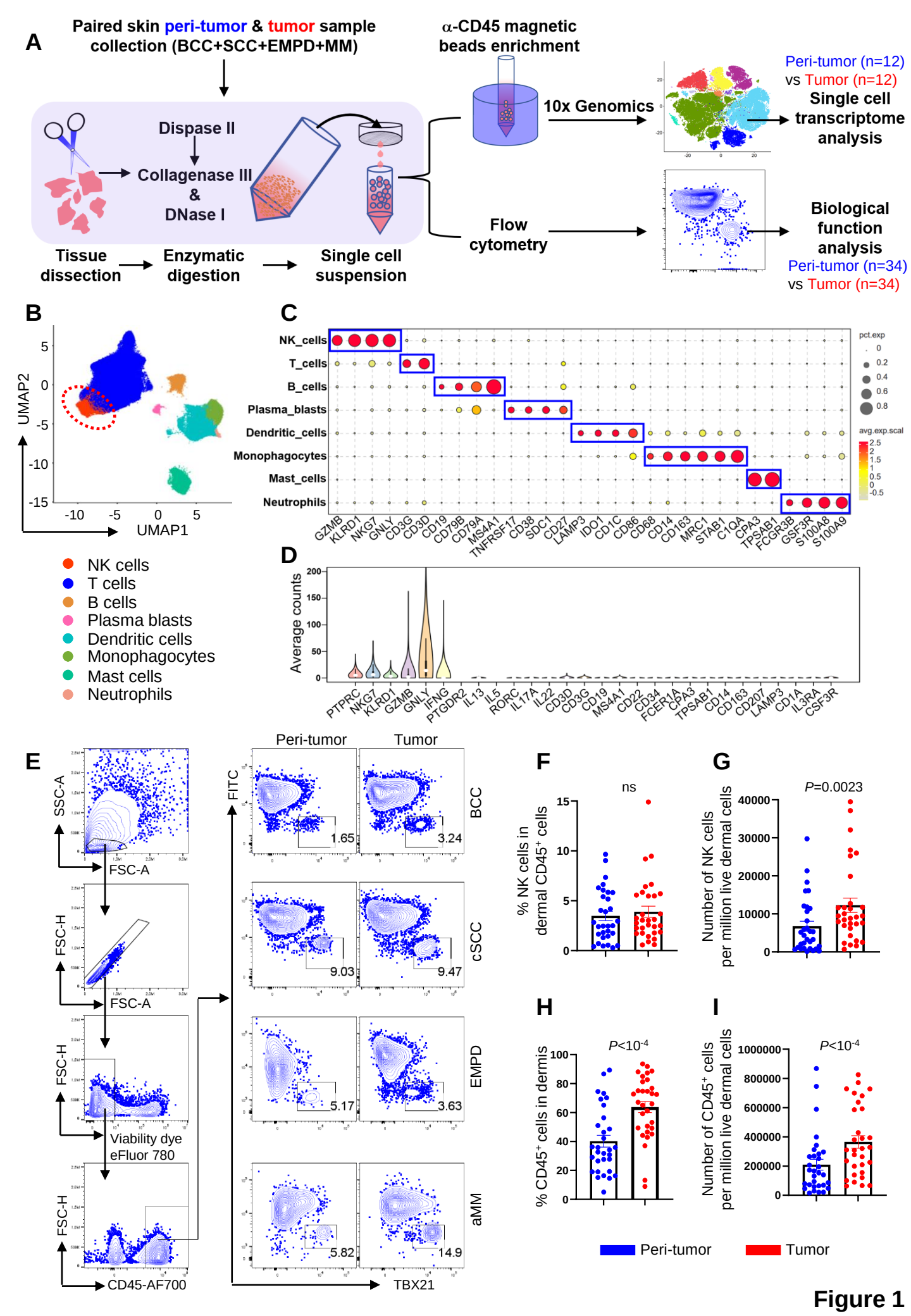
A
Paired skin peri-tumor & tumor sample collection (BCC+SCC+EMPD+MM)
Dispase II
Collagenase III & DNase I
Tissue dissection
Enzymatic digestion
Single cell suspension
α-CD45 magnetic beads enrichment
10x Genomics
Peri-tumor (n=12) vs Tumor (n=12)
Single cell transcriptome analysis
Flow cytometry
Biological function analysis
Peri-tumor (n=34) vs Tumor (n=34)
B
UMAP2
UMAP1
NK cells
T cells
B cells
Plasma blasts
Dendritic cells
Monophagocytes
Mast cells
Neutrophils
C
NK_cells
T_cells
B_cells
Plasma_blasts
Dendritic_cells
Monophagocytes
Mast_cells
Neutrophils
GZMB KLRD1 NKG7 GNLY CD3G CD3D CD19 CD79B CD79A MS4A1 TNFRSF17 CD38 SDC1 CD27 LAMP3 IDO1 CD1C CD86 CD68 CD14 CD163 MRC1 STAB1 C1QA CPA3 TPSAB1 FCGR3B GSF3R S100A8 S100A9
pct.exp
avg.exp.scal
D
Average counts
PTPRC NKG7 KLRD1 GZMB GNLY IFNG PTGDR2 IL13 IL5 RORC IL17A IL22 CD3D CD3G CD19 MS4A1 CD22 CD34 FCER1A CPA3 TPSAB1 CD14 CD163 CD207 LAMP3 CD1A IL3RA CSF3R
E
SSC-A
FSC-A
FSC-H
Viability dye eFluor 780
CD45-AF700
Peri-tumor
Tumor
FITC
TBX21
BCC
cSCC
EMPD
aMM
1.65
3.24
9.03
9.47
5.17
3.63
5.82
14.9
F
ns
% NK cells in dermal CD45+ cells
G
P=0.0023
Number of NK cells per million live dermal cells
H
P<10-4
% CD45+ cells in dermis
I
P<10-4
Number of CD45+ cells per million live dermal cells
Peri-tumor
Tumor

Figure 1

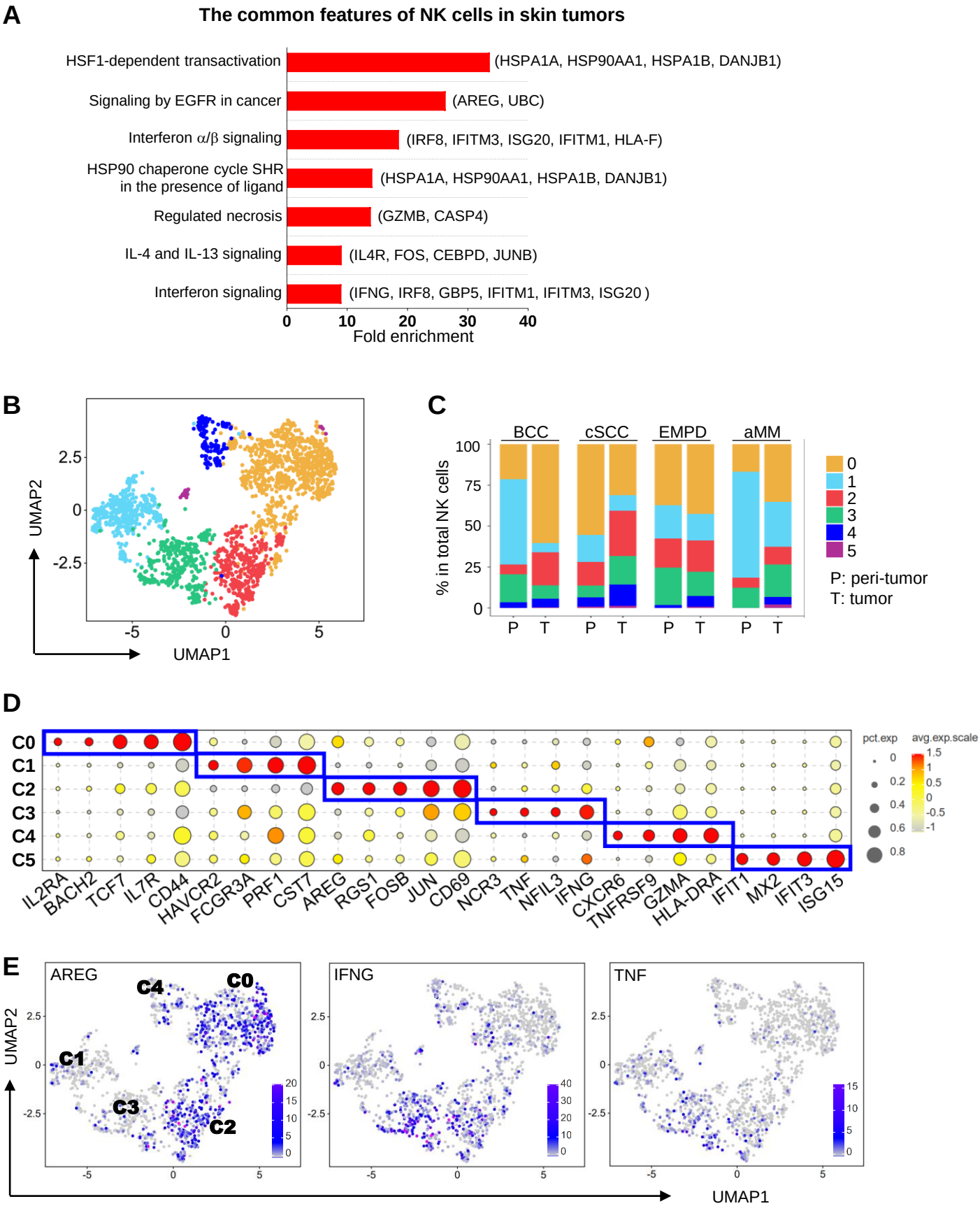
A
The common features of NK cells in skin tumors
HSF1-dependent transactivation
(HSPA1A, HSP90AA1, HSPA1B, DANJB1)
Signaling by EGFR in cancer
(AREG, UBC)
Interferon α/β signaling
(IRF8, IFITM3, ISG20, IFITM1, HLA-F)
HSP90 chaperone cycle SHR in the presence of ligand
(HSPA1A, HSP90AA1, HSPA1B, DANJB1)
Regulated necrosis
(GZMB, CASP4)
IL-4 and IL-13 signaling
(IL4R, FOS, CEBPD, JUNB)
Interferon signaling
(IFNG, IRF8, GBP5, IFITM1, IFITM3, ISG20)
0
10
20
30
40
Fold enrichment
B
UMAP2
UMAP1
C
BCC
cSCC
EMPD
aMM
% in total NK cells
P
T
0
1
2
3
4
5
P: peri-tumor
T: tumor
D
C0
C1
C2
C3
C4
C5
IL2RA
BACH2
TCF7
IL7R
CD44
HAVCR2
FCGR3A
PRF1
CST7
AREG
RGS1
FOSB
JUN
CD69
NCR3
TNF
NFIL3
IFNG
CXCR6
TNFRSF9
GZMA
HLA-DRA
IFIT1
MX2
IFIT3
ISG15
pct.exp
avg.exp.scale
E
AREG
IFNG
TNF
C0
C1
C2
C3
C4
UMAP2
UMAP1

Figure 2

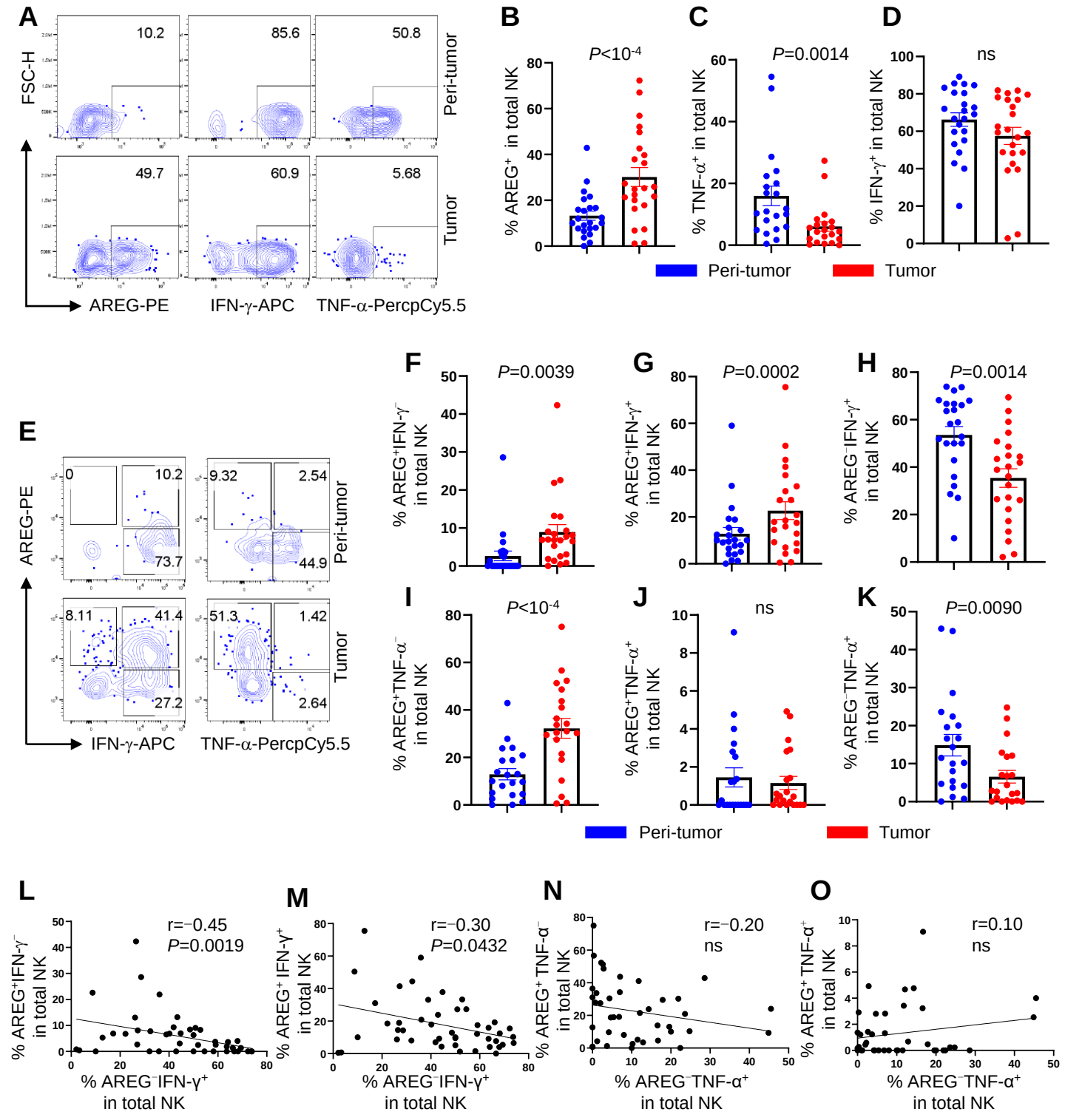
A
FSC-H
10.2
85.6
50.8
Peri-tumor
49.7
60.9
5.68
Tumor
AREG-PE
IFN-γ-APC
TNF-α-PercpCy5.5
B
P<10-4
% AREG+ in total NK
C
P=0.0014
% TNF-α+ in total NK
D
ns
% IFN-γ+ in total NK
Peri-tumor
Tumor
E
AREG-PE
0
10.2
73.7
9.32
2.54
44.9
8.11
41.4
27.2
51.3
1.42
2.64
IFN-γ-APC
TNF-α-PercpCy5.5
F
P=0.0039
% AREG+IFN-γ- in total NK
G
P=0.0002
% AREG+IFN-γ+ in total NK
H
P=0.0014
% AREG-IFN-γ+ in total NK
I
P<10-4
% AREG+TNF-α- in total NK
J
ns
% AREG+TNF-α+ in total NK
K
P=0.0090
% AREG-TNF-α+ in total NK
Peri-tumor
Tumor
L
r=−0.45
P=0.0019
% AREG+IFN-γ- in total NK
% AREG-IFN-γ+ in total NK
M
r=−0.30
P=0.0432
% AREG+ IFN-γ+ in total NK
% AREG-IFN-γ+ in total NK
N
r=−0.20
ns
% AREG+ TNF-α- in total NK
% AREG-TNF-α+ in total NK
O
r=0.10
ns
% AREG+ TNF-α+ in total NK
% AREG-TNF-α+ in total NK

Figure 3

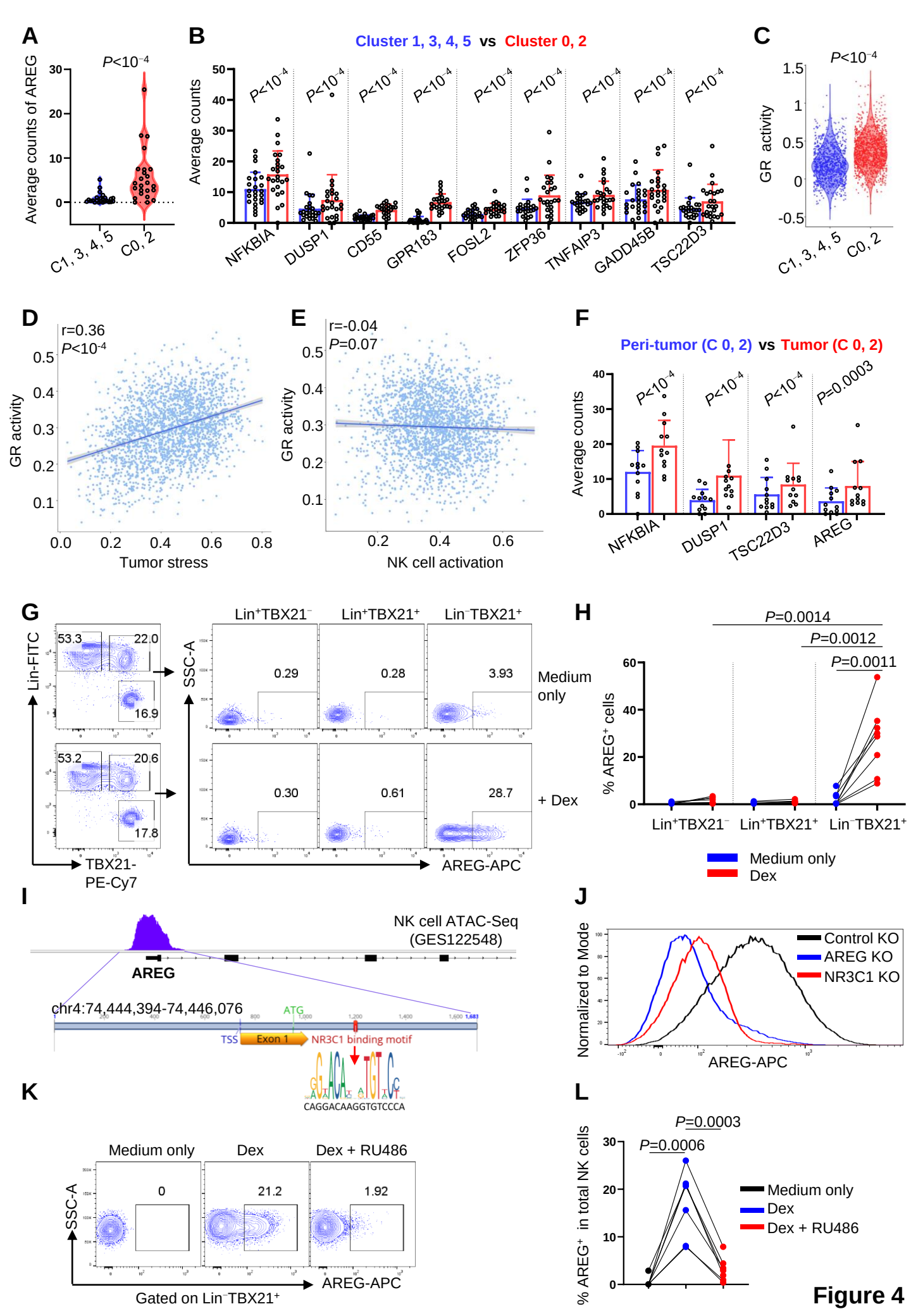
A
Average counts of AREG
P<10⁻⁴
C1, 3, 4, 5
C0, 2
B
Cluster 1, 3, 4, 5 vs Cluster 0, 2
Average counts
NFKBIA
DUSP1
CD55
GPR183
FOSL2
ZFP36
TNFAIP3
GADD45B
TSC22D3
C
GR activity
D
r=0.36
P<10⁻⁴
GR activity
Tumor stress
E
r=-0.04
P=0.07
GR activity
NK cell activation
F
Peri-tumor (C 0, 2) vs Tumor (C 0, 2)
Average counts
P=0.0003
AREG
G
Lin⁺TBX21⁻
Lin⁺TBX21⁺
Lin⁻TBX21⁺
Lin-FITC
TBX21-PE-Cy7
SSC-A
AREG-APC
Medium only
+ Dex
H
P=0.0014
P=0.0012
P=0.0011
% AREG⁺ cells
Medium only
Dex
I
NK cell ATAC-Seq (GES122548)
AREG
chr4:74,444,394-74,446,076
ATG
TSS
Exon 1
NR3C1 binding motif
CAGGACAAGGTGTCCCA
J
Normalized to Mode
Control KO
AREG KO
NR3C1 KO
AREG-APC
K
Medium only
Dex
Dex + RU486
SSC-A
AREG-APC
Gated on Lin⁻TBX21⁺
L
P=0.0003
P=0.0006
% AREG⁺ in total NK cells
Medium only
Dex
Dex + RU486

Figure 4

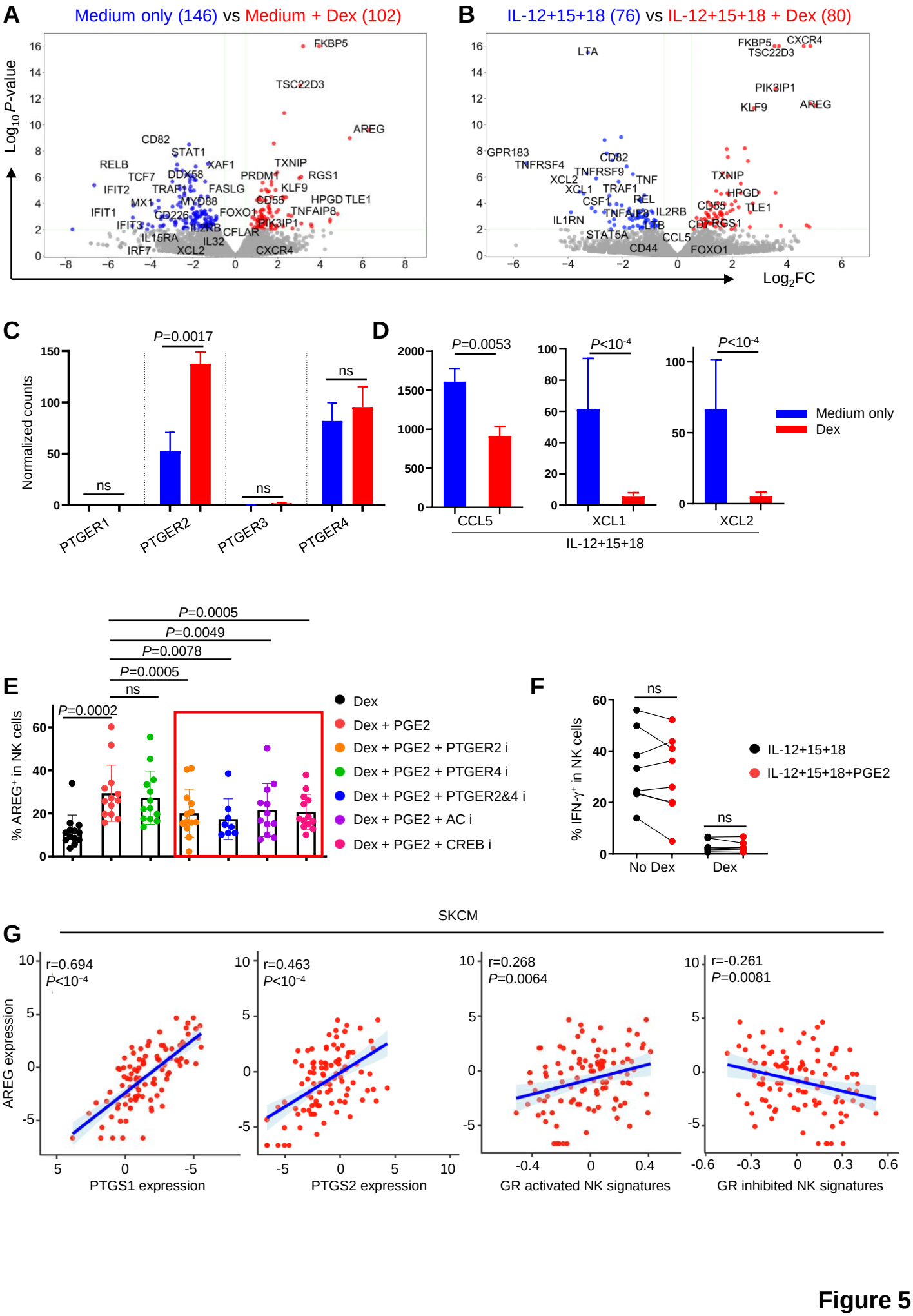
A
Medium only (146) vs Medium + Dex (102)
Log10 P-value
FKBP5
TSC22D3
AREG
CD82
STAT1
RELB
XAF1
TXNIP
TCF7
DDX58
PRDM1
RGS1
IFIT2
TRAF1
FASLG
KLF9
MX1
MYD88
CD55
HPGD
TLE1
IFIT1
CD226
FOXO1
TNFAIP8
IFIT3
IL2RB
PIK3IP1
CFLAR
IL15RA
IL32
IRF7
XCL2
CXCR4
B
IL-12+15+18 (76) vs IL-12+15+18 + Dex (80)
LTA
FKBP5
CXCR4
TSC22D3
PIK3IP1
KLF9
AREG
GPR183
CD82
TNFRSF4
TNFRSF9
XCL2
TNF
TXNIP
XCL1
TRAF1
HPGD
CSF1
REL
CD55
TLE1
IL1RN
TNFAIP3
IL2RB
LTB
CD7
RGS1
STAT5A
CCL5
CD44
FOXO1
Log2FC
C
P=0.0017
ns
ns
ns
Normalized counts
PTGER1
PTGER2
PTGER3
PTGER4
D
P=0.0053
P<10-4
P<10-4
CCL5
XCL1
XCL2
IL-12+15+18
Medium only
Dex
E
P=0.0005
P=0.0049
P=0.0078
P=0.0005
ns
P=0.0002
% AREG+ in NK cells
Dex
Dex + PGE2
Dex + PGE2 + PTGER2 i
Dex + PGE2 + PTGER4 i
Dex + PGE2 + PTGER2&4 i
Dex + PGE2 + AC i
Dex + PGE2 + CREB i
F
ns
ns
% IFN-γ+ in NK cells
IL-12+15+18
IL-12+15+18+PGE2
No Dex
Dex
G
SKCM
r=0.694
P<10-4
r=0.463
P<10-4
r=0.268
P=0.0064
r=-0.261
P=0.0081
AREG expression
PTGS1 expression
PTGS2 expression
GR activated NK signatures
GR inhibited NK signatures

Figure 5

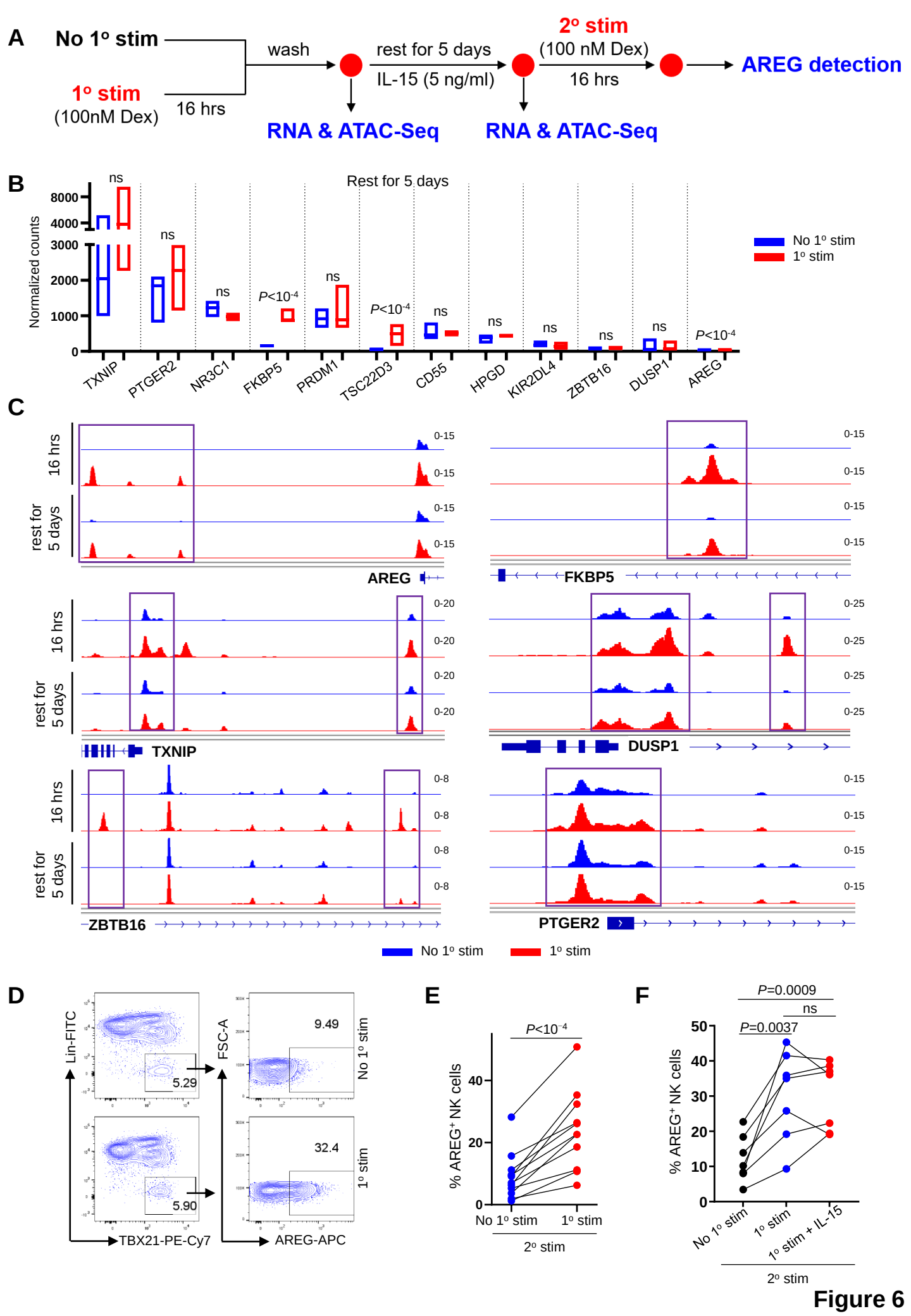
A
No 1º stim
1º stim
(100nM Dex)
16 hrs
wash
rest for 5 days
IL-15 (5 ng/ml)
2º stim
(100 nM Dex)
16 hrs
AREG detection
RNA & ATAC-Seq
RNA & ATAC-Seq
B
Rest for 5 days
Normalized counts
No 1º stim
1º stim
TXNIP
PTGER2
NR3C1
FKBP5
PRDM1
TSC22D3
CD55
HPGD
KIR2DL4
ZBTB16
DUSP1
AREG
C
16 hrs
rest for 5 days
AREG
FKBP5
TXNIP
DUSP1
ZBTB16
PTGER2
No 1º stim
1º stim
D
Lin-FITC
FSC-A
TBX21-PE-Cy7
AREG-APC
No 1º stim
1º stim
9.49
5.29
32.4
5.90
E
% AREG+ NK cells
No 1º stim
1º stim
2º stim
F
% AREG+ NK cells
No 1º stim
1º stim
1º stim + IL-15
2º stim

Figure 6

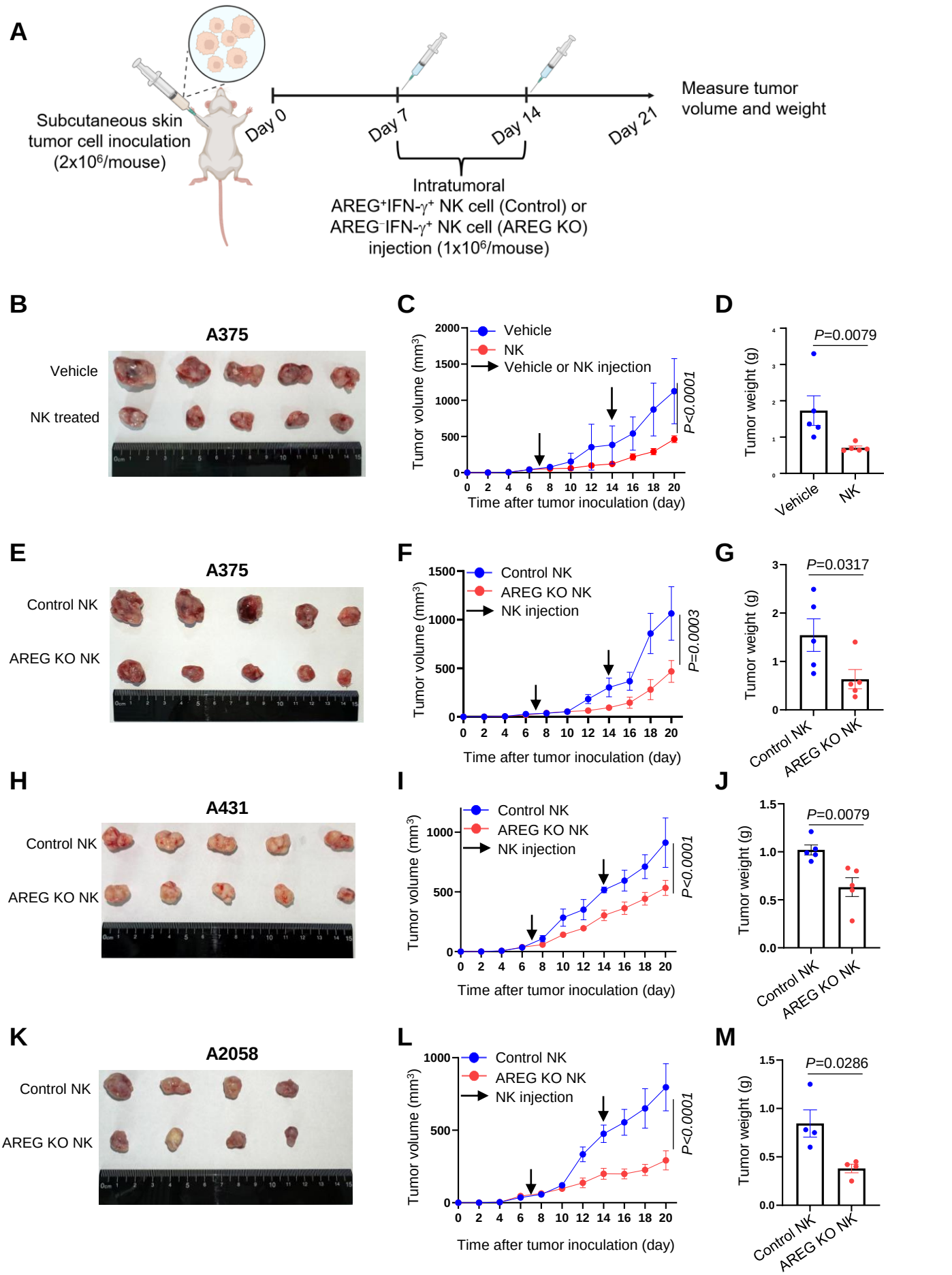
A
Subcutaneous skin tumor cell inoculation (2x10⁶/mouse)
Day 0
Day 7
Day 14
Day 21
Measure tumor volume and weight
Intratumoral AREG⁺IFN-γ⁺ NK cell (Control) or AREG⁻IFN-γ⁺ NK cell (AREG KO) injection (1x10⁶/mouse)
B
A375
Vehicle
NK treated
C
Vehicle
NK
Vehicle or NK injection
Tumor volume (mm³)
Time after tumor inoculation (day)
P<0.0001
D
P=0.0079
Tumor weight (g)
Vehicle
NK
E
A375
Control NK
AREG KO NK
F
Control NK
AREG KO NK
NK injection
Tumor volume (mm³)
Time after tumor inoculation (day)
P=0.0003
G
P=0.0317
Tumor weight (g)
Control NK
AREG KO NK
H
A431
Control NK
AREG KO NK
I
Control NK
AREG KO NK
NK injection
Tumor volume (mm³)
Time after tumor inoculation (day)
P<0.0001
J
P=0.0079
Tumor weight (g)
Control NK
AREG KO NK
K
A2058
Control NK
AREG KO NK
L
Control NK
AREG KO NK
NK injection
Tumor volume (mm³)
Time after tumor inoculation (day)
P<0.0001
M
P=0.0286
Tumor weight (g)
Control NK
AREG KO NK

Figure 7

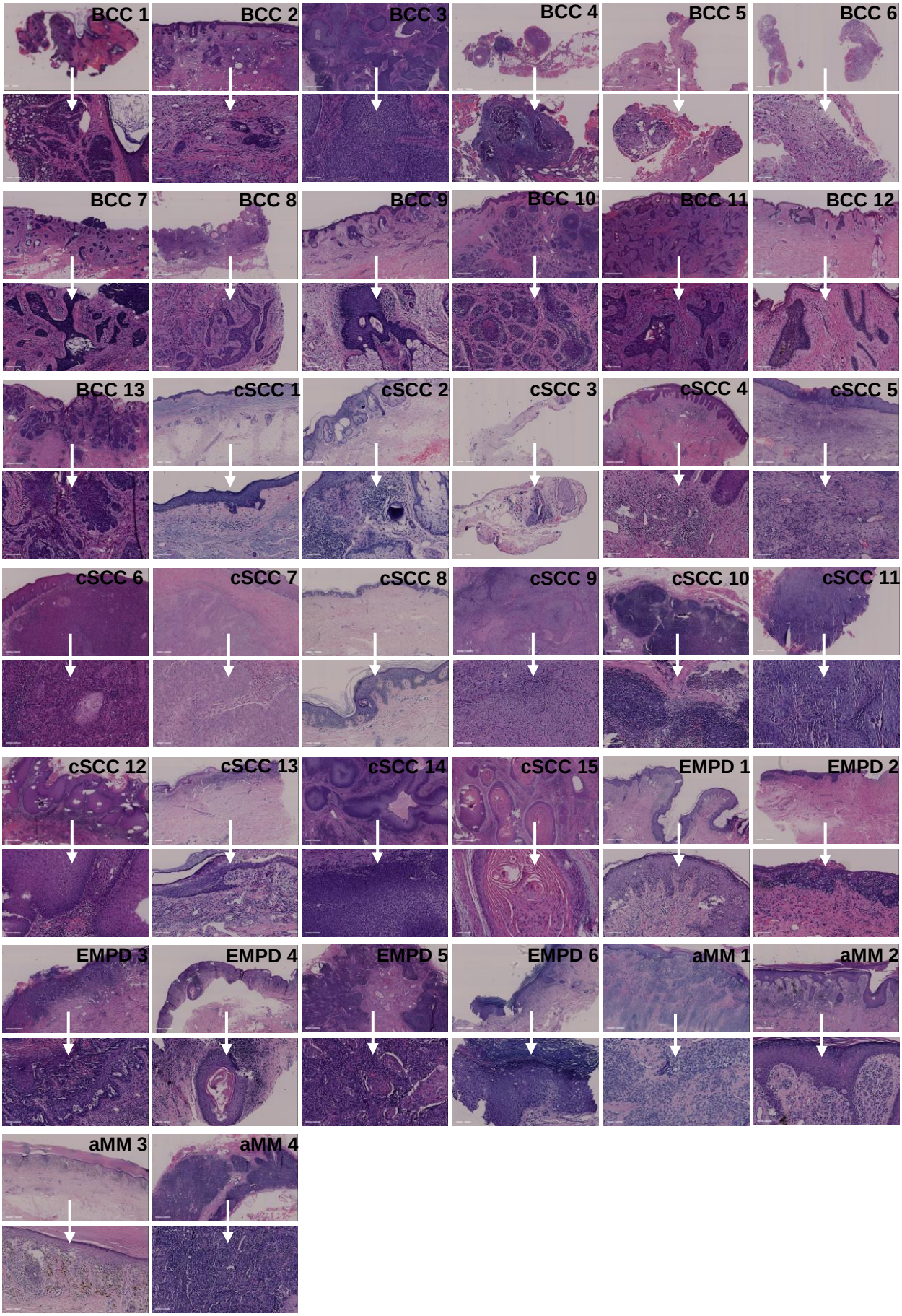
BCC 1
BCC 2
BCC 3
BCC 4
BCC 5
BCC 6
BCC 7
BCC 8
BCC 9
BCC 10
BCC 11
BCC 12
BCC 13
cSCC 1
cSCC 2
cSCC 3
cSCC 4
cSCC 5
cSCC 6
cSCC 7
cSCC 8
cSCC 9
cSCC 10
cSCC 11
cSCC 12
cSCC 13
cSCC 14
cSCC 15
EMPD 1
EMPD 2
EMPD 3
EMPD 4
EMPD 5
EMPD 6
aMM 1
aMM 2
aMM 3
aMM 4

Figure S1

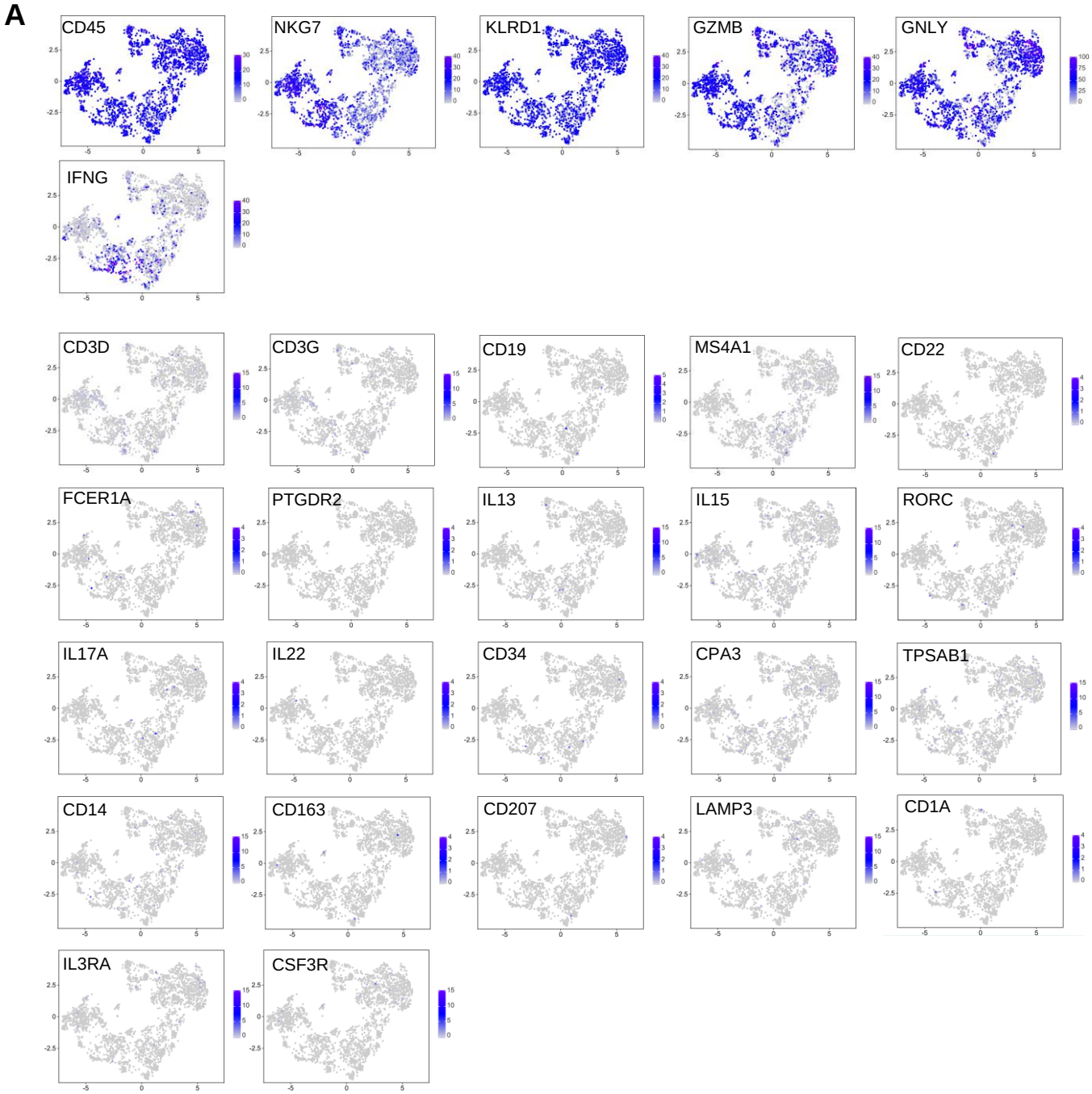
A
CD45
NKG7
KLRD1
GZMB
GNLY
IFNG
CD3D
CD3G
CD19
MS4A1
CD22
FCER1A
PTGDR2
IL13
IL15
RORC
IL17A
IL22
CD34
CPA3
TPSAB1
CD14
CD163
CD207
LAMP3
CD1A
IL3RA
CSF3R

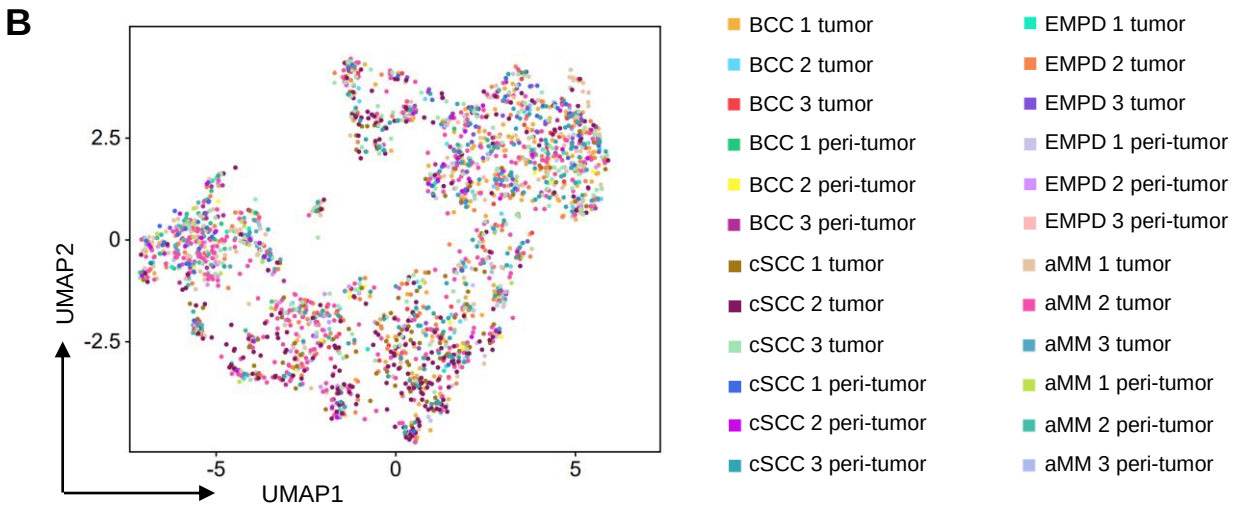
B
UMAP2
UMAP1
2.5
0
-2.5
-5
0
5
BCC 1 tumor
BCC 2 tumor
BCC 3 tumor
BCC 1 peri-tumor
BCC 2 peri-tumor
BCC 3 peri-tumor
cSCC 1 tumor
cSCC 2 tumor
cSCC 3 tumor
cSCC 1 peri-tumor
cSCC 2 peri-tumor
cSCC 3 peri-tumor
EMPD 1 tumor
EMPD 2 tumor
EMPD 3 tumor
EMPD 1 peri-tumor
EMPD 2 peri-tumor
EMPD 3 peri-tumor
aMM 1 tumor
aMM 2 tumor
aMM 3 tumor
aMM 1 peri-tumor
aMM 2 peri-tumor
aMM 3 peri-tumor

Figure S2

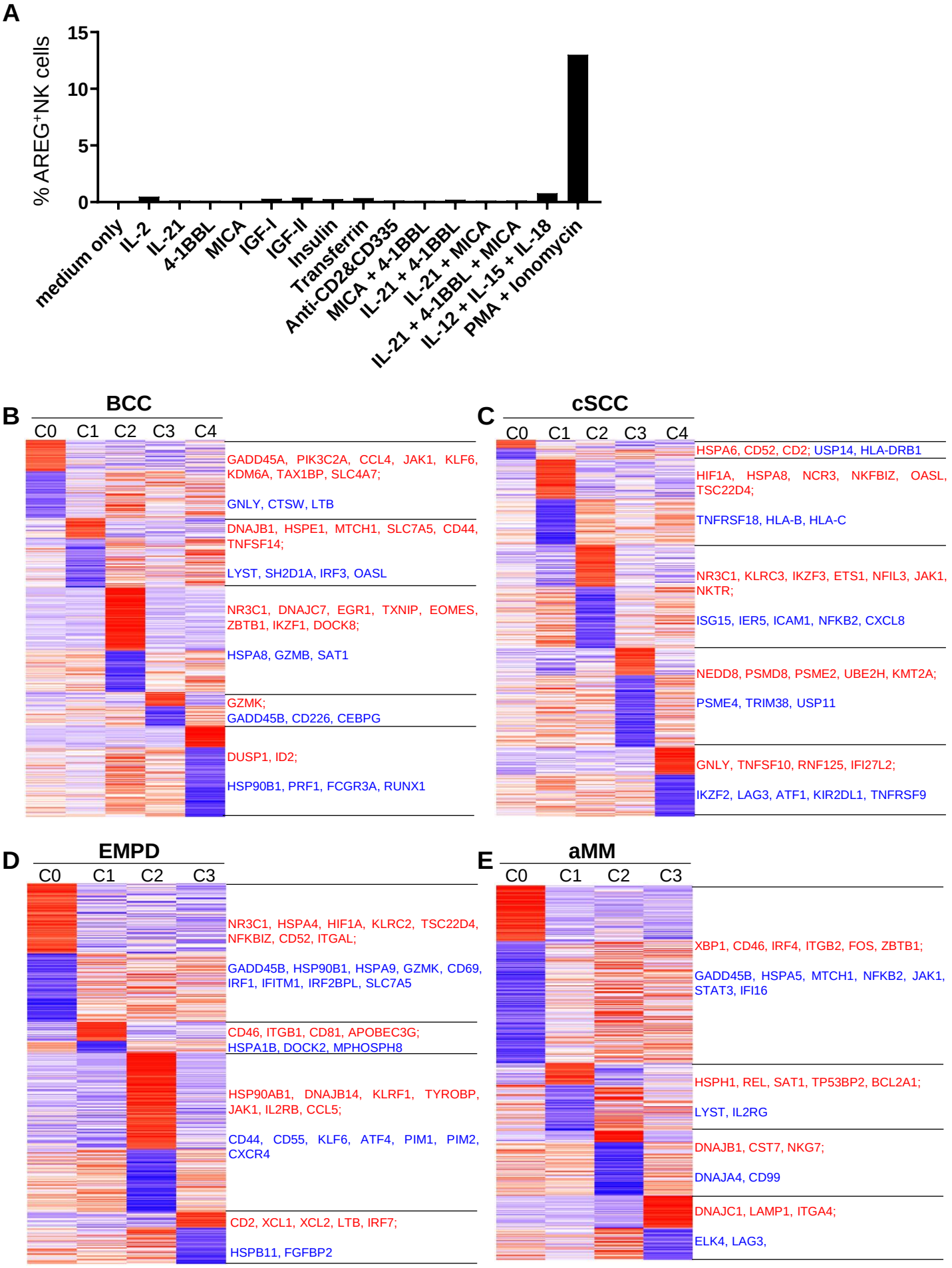
A
% AREG+NK cells
15
10
5
0
medium only
IL-2
IL-21
4-1BBL
MICA
IGF-I
IGF-II
Insulin
Transferrin
Anti-CD2&CD335
MICA + 4-1BBL
IL-21 + 4-1BBL
IL-21 + MICA
IL-21 + 4-1BBL + MICA
IL-12 + IL-15 + IL-18
PMA + Ionomycin
B
BCC
C0 C1 C2 C3 C4
GADD45A, PIK3C2A, CCL4, JAK1, KLF6, KDM6A, TAX1BP, SLC4A7;
GNLY, CTSW, LTB
DNAJB1, HSPE1, MTCH1, SLC7A5, CD44, TNFSF14;
LYST, SH2D1A, IRF3, OASL
NR3C1, DNAJC7, EGR1, TXNIP, EOMES, ZBTB1, IKZF1, DOCK8;
HSPA8, GZMB, SAT1
GZMK;
GADD45B, CD226, CEBPG
DUSP1, ID2;
HSP90B1, PRF1, FCGR3A, RUNX1
C
cSCC
C0 C1 C2 C3 C4
HSPA6, CD52, CD2; USP14, HLA-DRB1
HIF1A, HSPA8, NCR3, NKFBIZ, OASL, TSC22D4;
TNFRSF18, HLA-B, HLA-C
NR3C1, KLRC3, IKZF3, ETS1, NFIL3, JAK1, NKTR;
ISG15, IER5, ICAM1, NFKB2, CXCL8
NEDD8, PSMD8, PSME2, UBE2H, KMT2A;
PSME4, TRIM38, USP11
GNLY, TNFSF10, RNF125, IFI27L2;
IKZF2, LAG3, ATF1, KIR2DL1, TNFRSF9
D
EMPD
C0 C1 C2 C3
NR3C1, HSPA4, HIF1A, KLRC2, TSC22D4, NFKBIZ, CD52, ITGAL;
GADD45B, HSP90B1, HSPA9, GZMK, CD69, IRF1, IFITM1, IRF2BPL, SLC7A5
CD46, ITGB1, CD81, APOBEC3G;
HSPA1B, DOCK2, MPHOSPH8
HSP90AB1, DNAJB14, KLRF1, TYROBP, JAK1, IL2RB, CCL5;
CD44, CD55, KLF6, ATF4, PIM1, PIM2, CXCR4
CD2, XCL1, XCL2, LTB, IRF7;
HSPB11, FGFBP2
E
aMM
C0 C1 C2 C3
XBP1, CD46, IRF4, ITGB2, FOS, ZBTB1;
GADD45B, HSPA5, MTCH1, NFKB2, JAK1, STAT3, IFI16
HSPH1, REL, SAT1, TP53BP2, BCL2A1;
LYST, IL2RG
DNAJB1, CST7, NKG7;
DNAJA4, CD99
DNAJC1, LAMP1, ITGA4;
ELK4, LAG3,

Figure S3

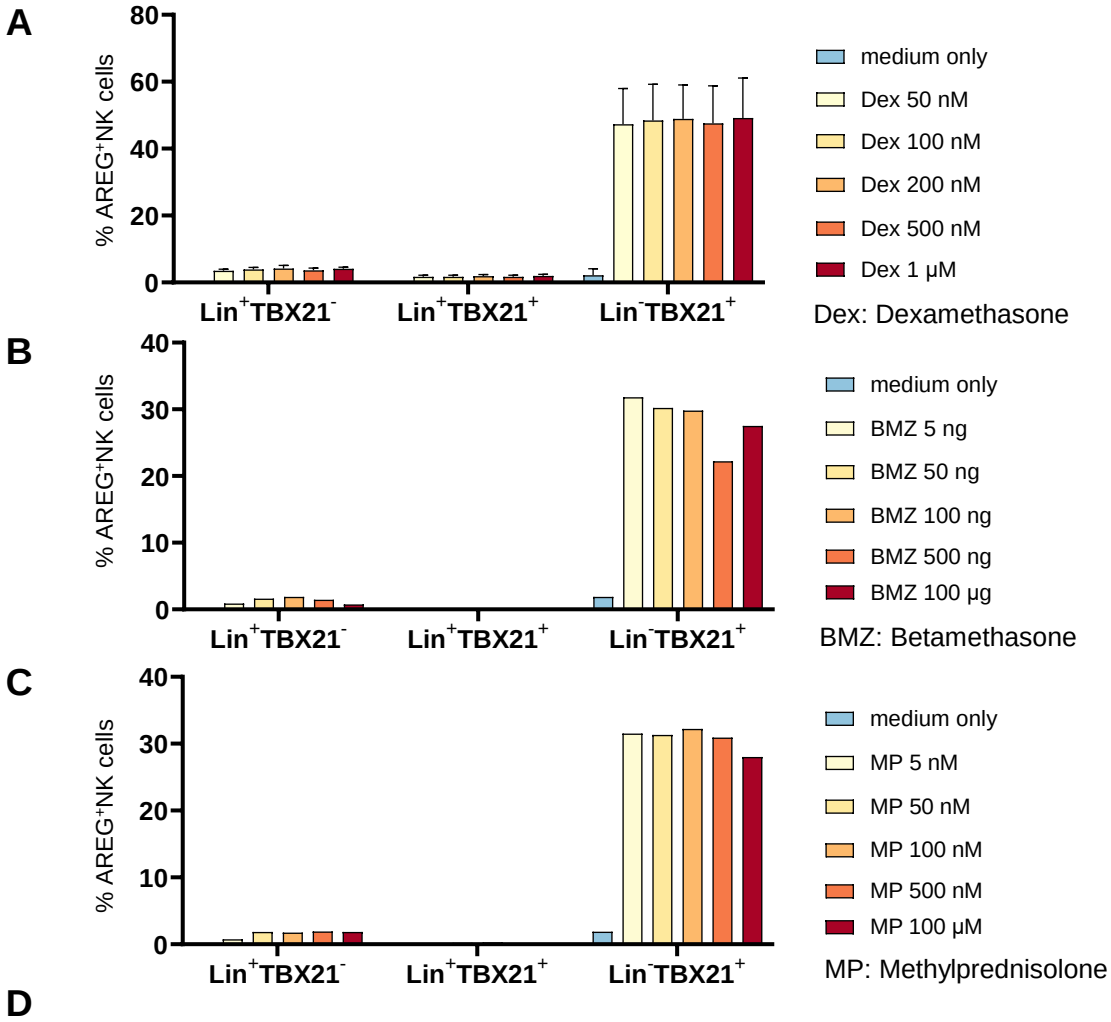
A
% AREG+NK cells
80
60
40
20
0
Lin+TBX21-
Lin+TBX21+
Lin-TBX21+
medium only
Dex 50 nM
Dex 100 nM
Dex 200 nM
Dex 500 nM
Dex 1 μM
Dex: Dexamethasone
B
% AREG+NK cells
40
30
20
10
0
Lin+TBX21-
Lin+TBX21+
Lin-TBX21+
medium only
BMZ 5 ng
BMZ 50 ng
BMZ 100 ng
BMZ 500 ng
BMZ 100 μg
BMZ: Betamethasone
C
% AREG+NK cells
40
30
20
10
0
Lin+TBX21-
Lin+TBX21+
Lin-TBX21+
medium only
MP 5 nM
MP 50 nM
MP 100 nM
MP 500 nM
MP 100 μM
MP: Methylprednisolone

D

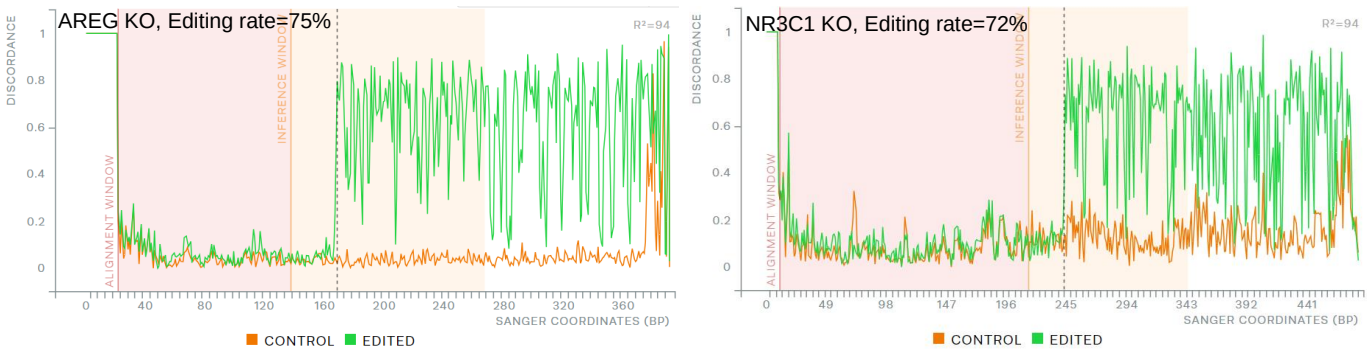
AREG KO, Editing rate=75%
DISCORDANCE
ALIGNMENT WINDOW
INFERENCE WINDOW
R²=94
SANGER COORDINATES (BP)
CONTROL
EDITED
NR3C1 KO, Editing rate=72%
DISCORDANCE
ALIGNMENT WINDOW
INFERENCE WINDOW
R²=94
SANGER COORDINATES (BP)
CONTROL
EDITED

Figure S4

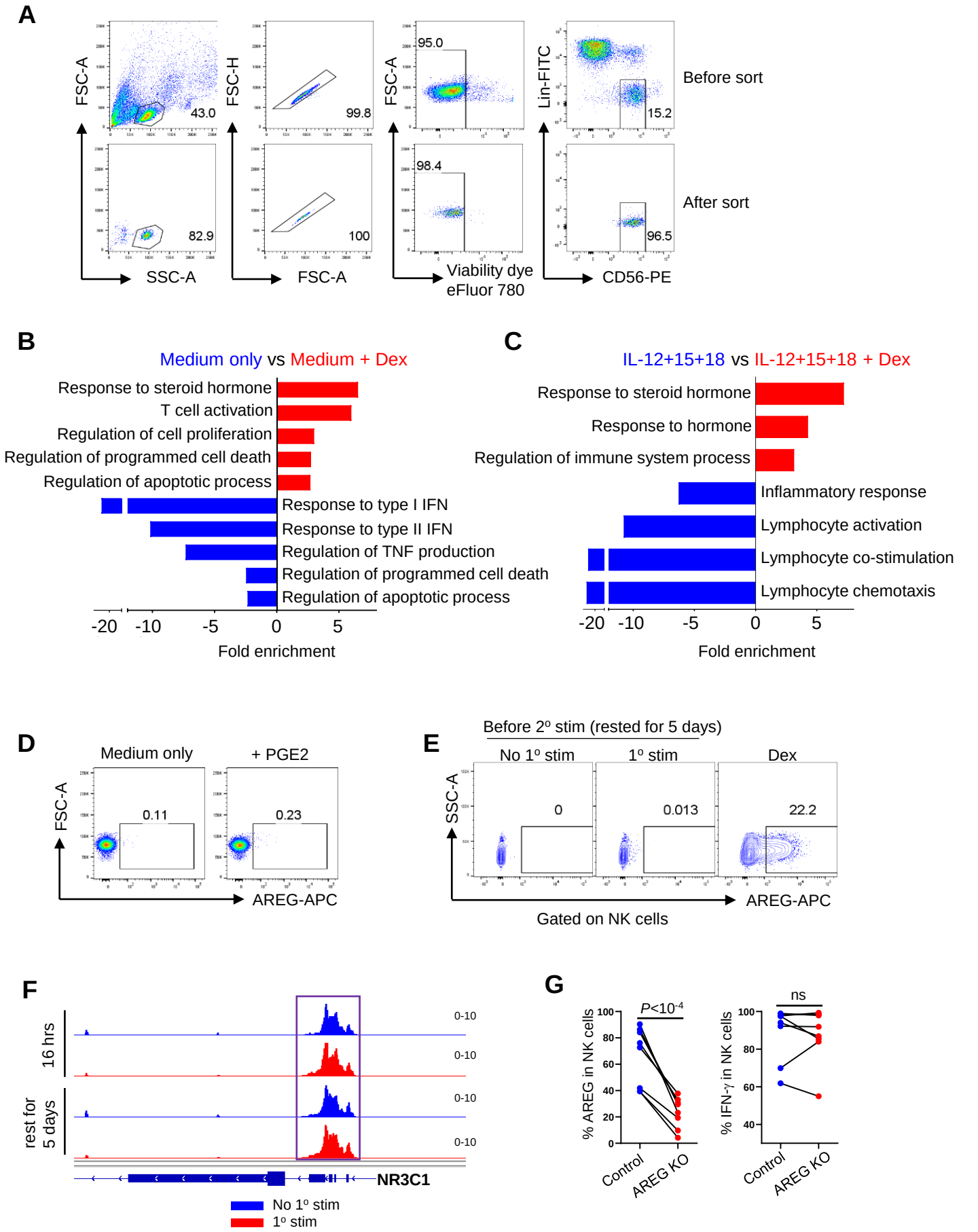
A
FSC-A
SSC-A
43.0
82.9
FSC-H
FSC-A
99.8
100
FSC-A
Viability dye eFluor 780
95.0
98.4
Lin-FITC
CD56-PE
15.2
96.5
Before sort
After sort
B
Medium only vs Medium + Dex
Response to steroid hormone
T cell activation
Regulation of cell proliferation
Regulation of programmed cell death
Regulation of apoptotic process
Response to type I IFN
Response to type II IFN
Regulation of TNF production
Regulation of programmed cell death
Regulation of apoptotic process
-20 -10 -5 0 5
Fold enrichment
C
IL-12+15+18 vs IL-12+15+18 + Dex
Response to steroid hormone
Response to hormone
Regulation of immune system process
Inflammatory response
Lymphocyte activation
Lymphocyte co-stimulation
Lymphocyte chemotaxis
-20 -10 -5 0 5
Fold enrichment
D
Medium only
+ PGE2
FSC-A
0.11
0.23
AREG-APC
E
Before 2º stim (rested for 5 days)
No 1º stim
1º stim
Dex
SSC-A
0
0.013
22.2
AREG-APC
Gated on NK cells
F
16 hrs
rest for 5 days
0-10
NR3C1
No 1º stim
1º stim
G
% AREG in NK cells
P<10-4
Control
AREG KO
% IFN-γ in NK cells
ns
Control
AREG KO

Figure S5

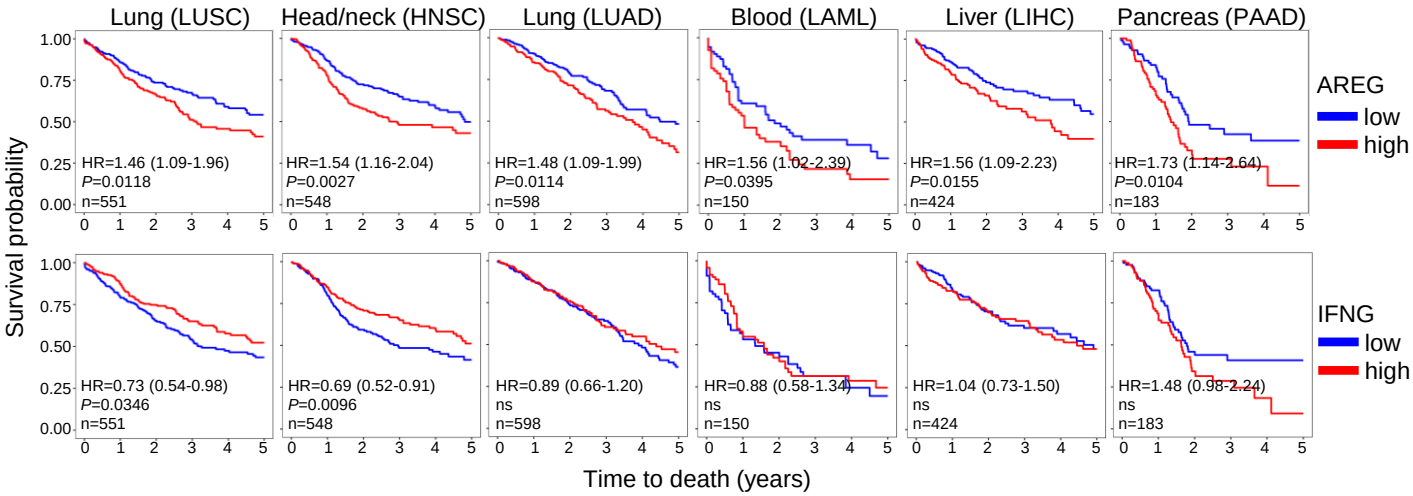
Lung (LUSC)
Head/neck (HNSC)
Lung (LUAD)
Blood (LAML)
Liver (LIHC)
Pancreas (PAAD)
Survival probability
1.00
0.75
0.50
0.25
0.00
HR=1.46 (1.09-1.96)
P=0.0118
n=551
HR=1.54 (1.16-2.04)
P=0.0027
n=548
HR=1.48 (1.09-1.99)
P=0.0114
n=598
HR=1.56 (1.02-2.39)
P=0.0395
n=150
HR=1.56 (1.09-2.23)
P=0.0155
n=424
HR=1.73 (1.14-2.64)
P=0.0104
n=183
AREG
low
high
HR=0.73 (0.54-0.98)
P=0.0346
n=551
HR=0.69 (0.52-0.91)
P=0.0096
n=548
HR=0.89 (0.66-1.20)
ns
n=598
HR=0.88 (0.58-1.34)
ns
n=150
HR=1.04 (0.73-1.50)
ns
n=424
HR=1.48 (0.98-2.24)
ns
n=183
IFNG
low
high
0 1 2 3 4 5
Time to death (years)

Figure S6